

Depositional environment of the surface sediments in Central Indian Basin (CIB), Indian Ocean, between 8⁰- 18⁰S latitude and 72⁰-79⁰E longitude, based on their geochemical characteristics

Simontini Sensarma^{1*}, Ranadip Banerjee¹, Manavalan Satyanarayanan ², Subir Mukhopadhyay³.

¹CSIR-National Institute of Oceanography, Dona Paula, Goa-403004.

²CSIR-National Geophysical Research Institute, Uppal Road, Hyderabad-500606;

³Jadavpur University, Kolkata-700032, West Bengal.

*Corresponding author : Simontini Sensarma,

Email: simontinisensarma@gmail.com

Phone: +91 832-2450-244; Fax: +91 832-2450-609

Abstract

To establish the depositional environment of the surface sediments in the Central Indian Basin (CIB), Indian Ocean, major and trace element compositions of different sediment types were studied. The study area comprised of terrigenous-siliceous transition, calcareous, siliceous and red clay sediments. The sediment type changed due to various physico-chemical conditions with varying proportions of biogenic, hydrogenetic, early diagenetic and detrital inputs. An oxidative environment is present throughout the basin with variable intensity. The terrigenous input was variable in all sediment types, while its signature was traceable up to 15.30⁰S latitude. The variable distribution pattern of Mn_{excess} and Fe_{excess} indicate that apart from continental source, there were additional sources of supply for both these elements, with which most of the trace metals like nickel, copper, chromium, vanadium, yttrium, rubidium and thorium were associated. The Al/Ti ratios of the sediments indicate a terrestrial influence of fluvial nature upto as far as 14⁰S latitude while, in the calcareous zone, the influence of volcanic precursors was observed. The present study envisages that Al_{excess} in the sediments adjacent to the ridges and fracture zones might indicate that Al in these areas is not entirely derived from the continental source.

Keywords: Indian Ocean, Central Indian Basin, deep-sea, sediments, geochemistry, major elements

1. Introduction:

The sedimentation pattern of a basin is affected by a number of varying depositional conditions like its morphology, surface-water productivity, bottom-water current etc. In terms of those, the Central Indian Basin (CIB) in the Indian Ocean has a very complicated geo-morphic set up. It is bounded by ridge systems on three sides (western, eastern and southern) and receives a heavy continental input from the north due to the presence of Ganga-Brahmaputra delta system (Borole 1993; Banerjee, 1998; Pattan et al, 2005; Valsangkar, 2000, 2011). Moreover, high biological productivity in the surface waters of this basin at around 10°S latitude (Parsons et al, 1977) and presence of a vast manganese nodule field (Nath et al, 1989; Vineesh et al., 2009) have made the geochemical study of surface sediments of the CIB an important subject of interest. Apart from this, the existences of a number of seamounts and fracture zones have also been reported in the basin area of the CIB (Kamesh Raju, 1993; Kamesh Raju et al, 1993; Kodagali et al, 1992).

The CIB sediments can be broadly classified into four major types: (i) terrigenous, (ii) calcareous, (iii) siliceous and (iv) red clay (or pelagic clay). Grain size analysis of these sediments shows that they are mainly silty in nature, with mean grain size ($M_{2\phi}$) of 7.0-8.6 μ m for surface and 6.6-8.6 μ m for subsurface sediment (Mukhopadhyay et al, 2008). Illite, kaolinite and chlorite are the major clay minerals present in these sediments indicating continental influence. However, iron-rich montmorillonite is also found in the <1 and 1-2 μ m fractions of these sediments, which might have formed due to the interaction of biogenic silica with the iron oxyhydroxides (Mukhopadhyay et al, 2008). The coarse fractions of these sediments (>63 μ m grain size) were mainly composed of planktonic shells, glass shards, pumice and palagonite fragments, micronodules and other rock and mineral fragments. The distribution of calcium carbonate (Kolla et al, 1976), mineralogy and geochemistry of surface sediments (Rao and Nath 1988, Nath et al., 1989, Banerjee, 1998), distribution of biogenic silica (Pattan et al., 1992) erosion of surface sediment due to activity of Antarctic Bottom Water (AABW) (Vineesh et al., 2009) and sedimentation history (Borole, 1993) from different parts of this basin have been discussed by earlier workers. In comparison to the equatorial Pacific, these data are not enough with reference to several other parameters (e.g. redox condition of the sediments, extent of terrigenous supply, source of some major metals and their interrelationship with the trace metals etc.) related to the metal distribution pattern and enrichment processes in the CIB area.

Thus, in the present study, the following objectives have been undertaken for better understanding of the parameters which are yet to be studied in the CIB sediments:

- a) To establish the oxidation-reduction conditions of the CIB surface sediments.
- b) To study the detrital influence on these sediments using the distribution pattern of titanium and aluminium versus titanium ratio.
- c) To understand the behavior of excess aluminium, manganese and iron contents of the CIB surface sediments and their correlation with the trace metals like Ba, Sr, Cr, V, Ni, Cu, Th, Rb, Y, Nb, Pb, Zn, Zr and Sc.
- d) To study the excess opal and calcium contents of the CIB surface sediments along with their strontium and barium contents to understand their role as surface productivity indicators.

Using all the above mentioned parameters an attempt is made to summarize the overall sedimentary depositional environment in the CIB.

2. Materials and Methods:

2.1. Study area and sampling:

Surface sediment samples were collected from 69 locations in the CIB, broadly between 08⁰ and 18⁰S latitude and 72⁰ and 79⁰E longitude, mainly covering terrigenous-siliceous (T-S) transition sediment (6 samples), siliceous ooze (38 samples), red clay (20 samples) and calcareous ooze sediments (5 locations). Free fall grabs were used for surface sediment collection, with the sediment collection tube attached to the grabs alongwith four gravity cores whose topmost section (0-5cm) was used as the representative surface samples of those locations. These surface samples and cores were collected during several cruises of *ORV Sagarkanya* and *AA Sidorenko*, as a part of the "project surveys for polymetallic nodules" in the CIB. The sample locations and different sediment types are presented in Fig 1. After collection the sediments were washed thoroughly with deionized water, dried, powdered and stored in plastic containers at room temperature.

2.2 Major element analysis:

Each sample was hand ground into fine powder by an agate mortar and pestle for geochemical analyses of the bulk sediment samples. Splits of the powdered samples (0.55g) were then fused into borate glass beads at high temperature (1180°C) using Spectromelt® A12, Merck. These beads were then analyzed for the determination of major element oxide by using X-Ray Fluorescence Spectrometer (PANalytical, AXIOS®). Marine sediment JSd-1 was used as a standard reference material. The sediment types, locations and the major element concentrations of the samples are given in Table 1a.

2.3. Trace element analysis:

Thirty five representative samples were chosen for trace element analyses representing all sediment types. 50mg of each sample was treated with 15ml supra-pure acid mixture (HF:HNO₃:HClO₄ = 7:3:1) in Teflon beakers and then evaporated to dryness on a hot plate at 180°C. To this, 4ml (1:1) supra-pure nitric acid solution was added and the final volume was adjusted to 100ml with Milli-Q water. Marine reference standard material MAG-1 and JSd-1, along with a couple of procedural blanks, were also prepared with the sample batch by adopting the same protocol described above to negate errors due to reagent and handling. Trace element concentrations were then measured by an X-Series II (Thermo Fisher) quadrupole Inductively Coupled Plasma-Mass Spectrometer (ICP-MS), using ¹⁰³Rh solution (20ng/ml) as internal standard. Precision and accuracy were better than RSD 3% for the majority of trace elements. The sediment types and the trace element concentrations of the samples, selected for trace element analyses, are given in Table 2. The recovery of both major element oxides and trace elements, relative to the certified reference materials, is given in the Table 3.

2.4. Q-mode factor analysis:

The factor analysis of major element oxides and trace elements of the surface sediment samples under study was performed separately using C-2 data Analysis program by Steve Juggins (NORPAST, University of Bergen, Juggins, 2003; <https://www.staff.ncl.ac.uk/stephen.juggins/software/C2Home.htm>). The data was analysed for quality and continuity, and normalized by square root method before factor analysis to avoid biases of highly dominating percentages of certain elemental oxides. Q-mode Factor analysis revealed two significant factors for major element oxides and four for trace elements, explaining cumulative variance of 99.75% and 98.88% of the elemental information, respectively, retained in the Q-mode factor model.

3. Results:

3.1. Oxidation-reduction conditions:

To determine the oxidation-reduction conditions (Mn*) of the surface sediments the following equation was used after Machhour et al., (1994).

$$Mn^* = \log[(Mn_{\text{samples}}/Mn_{\text{shales}})/(Fe_{\text{samples}}/Fe_{\text{shales}})] \dots \dots \dots (1)$$

This equation gives an idea about the redox potential of the depositional environment. Positive value of Mn* indicates oxidizing environment and negative value means sub-oxic environment. The mean

values for Mn shales and Fe shales were taken from Wedepohl (1978). In the present case, all the samples fell within the oxidizing domain (Fig 2a). Calcareous and red clay sediments showed highest Mn* values while siliceous and terrigenous-siliceous transition (T-S) sediments showed lower values (Table 1b). One sample from siliceous sediment even showed negative value (-0.08 for station number 38/195). The Al and Mn contents of this sample are the lowest with corresponding highest biogenic silica content. Thus the low Mn* value of this sample is not due to the presence of higher amount of silicates, which intrinsically contains less Mn, but due to the higher biogenic silica which created a localized sub-oxic condition preventing further Mn re-deposition. Also from the sequential extraction studies of the surface sediment samples from this area, it was found out that the major metal binding phases were easily reducible Fe and Mn oxyhydroxides which are freshly precipitated in the system, indicating overall oxic condition (Sensarma et al, 2016). The dissolved oxygen in the sediment pore water from this area has been reported to be around 185µM at about 4000-5000m water depth (Mukhopadhyay et al., 2008), which indicates sufficiently oxic condition of the surface sediments.

Alternately, V/Cr ratio can also be applied for determining the redox condition of the sediment (Dill et al, 1988; Jones and Manning, 1994) where values >4.5 indicate anoxic environment and <2 means oxic environment. In case of the CIB sediments all the samples show values <2, and thus reconfirm that the surface sediments of the CIB were deposited in an oxic environment (Table 2). However, the red clay sediment on an average has higher V/Cr ratio ~1.96, than the other sediment types. Two of the siliceous ooze samples crossed the limiting value 2 of the oxic condition (38/3 and 38/4), indicating localized sub-oxic condition. Nonetheless, an overall oxidizing domain is considered in the study area and the localized sub-oxic condition was found only in the siliceous domain probably due to higher biogenic silica input.

3.2. Terrigenous Influence:

To detect the percentage of terrigenous matter, present in the sediments, the shale normalized titanium (Ti) concentration of the sediments can be used as an excellent proxy (Schroeder et al, 1997). Ti is mostly considered to be derived from continents with similar composition as that of Post Archean Australian Shale (PAAS) (Taylor and McLennan, 1985) and is most stable element under varying physico-chemical changes. The following equation (after Schroeder et al, 1997) was used here to determine the Terrigenous percentage (%) in CIB sediments:

$$\text{Terrigenous \%} = (\text{Ti}_{\text{total}} / \text{Ti}_{\text{PAAS}}) \times 100 \dots \dots \dots (2)$$

where the concentration of Ti in PAAS is 0.6 (wt%). Thus higher percentage of terrigenous matter will indicate more terrigenous influence. In the present study, lowest values of Terrigenous % were reported from calcareous sediment (average ~32.9%), followed by T-S sediment (average ~38.2%), siliceous sediment (average ~40.6%) and highest in red clay (average ~46.9%) (Fig 2b).

3.3. “Excess” Mn, Fe and Al in the sediments:

To determine the relative contributions of the terrigenous and non-terrigenous portions for iron and manganese, its “excess” i.e. non-terrigenous part is calculated from the following relationship, described by Schroeder et al. (1997).

$$El_{\text{excess}} = El_{\text{total}} - [Ti_{\text{total}} \times (El_{\text{PAAS}} / Ti_{\text{PAAS}})] \dots \dots \dots (3)$$

where El denotes element (Fe and Mn in this case). The PAAS value of Ti is already stated earlier and that of Fe and Mn are 5 and 0.085 (wt %), respectively (Taylor and McLennan, 1985). Mn_{excess} was highest in red clay, followed by calcareous sediment, then siliceous ooze and least in the T-S sediment (Fig 2c). The same distribution pattern was also found in case of Fe_{excess} (Table 1b, Fig 2d).

Similarly, to determine the excess or non-terrigenous source of Al, the following equation was used after Murray and Leinen, (1996),

$$Al(\text{excess}) = Al_{\text{total}} - (16.66 \times Ti_{\text{total}}) \dots \dots \dots (4)$$

where, 16.66 = Al/Ti ratio of PAAS (Taylor and McLennan, 1985). Following this method, all the samples showed some amount of excess aluminium. Interestingly, the samples near the ridge areas and fracture zones (close to 73⁰, 76⁰30', 79⁰E longitudes, comprising of calcareous and red clay), showed slightly higher concentration of Al_{excess} (average ~2.7% for both the sediment types) (Fig 3a). While, the samples further from these fracture zones (T-S and siliceous sediments) had much lesser amount of Al_{excess} (Table 1b).

3.4. Al/Ti ratio of the sediment samples:

The Al/Ti ratio can be used to indicate the non-biogenic particulate matter in marine sediments (Murdmaa et al., 1980). It has also been interpreted as an indicator of grain size change (Boyle, 1983) as Ti is known to be preferentially concentrated in heavy minerals like titanomagnetite, ilmenite, rutile etc., found in coarser sediments, whereas Al mainly comes from the aluminosilicates of clay minerals. In the present study, the Al/Ti ratio of the samples varied according to sediment type (Fig 3b). The average Al/Ti ratio of the T-S and siliceous sediments were 17.8 and 22.3 respectively, which is similar to the Pacific hemipelagic sediments (18 to 22; Murdmaa et al., 1980), while Al/Ti values of "average shale" and “modern river load of the world” are 17.5

(Boström, 1976) and 20.8 (Gordeev and Lisitzin, 1979) respectively. However, calcareous sediments showed higher Al/Ti ratio of 28.7 on average, which can be caused due to the influence of acidic, vitric ash and plagioclase (Murdmaa et al., 1980). On the other hand, all red clay sediments had Al/Ti ratio >22 with an average of 23.8 which is similar to upper continental crust value (23.7; Taylor and McLennan, 1985).

3.5. Surface Productivity indicators:

The depth of CCD in the CIB was never constant and varied between 4000 to 5050m over the geological past (Kolla et al, 1976). Sabine et al (2002) have reported that calcite saturation depth is around 3800m in the CIB with a much shallower aragonite saturation depth (~1000m). On the other hand, Banakar et al (1998) mentioned that the lysocline and carbonate compensation depth (CCD) in the CIB area lies within 4400-4700m of water depth. The total organic carbon (TOC) content of the CIB sediments vary from <0.05 to 1.54% while their total inorganic carbon (TIC) content vary from below detection limit upto 10% in calcareous oozes (Gupta and Jauhari, 1994; Das et al, 2011). A major part of this TIC comes from the dissolution of the calcareous test of marine planktons like coccoliths, forams etc. That is why, the samples from calcareous sediment showed highest concentration of CaO (average ~15.1%) which becomes negligible in all other sediment types (Table 1a). Siliceous and red clay sediments had average CaO concentrations of 1.09% and 1.32% respectively while, T-S sediment had the lowest concentration of 0.37% on average (Fig 3c). This kind of low concentration of CaO can also occur due to the alteration of feldspar and clay minerals which are abundant in the CIB sediments (Gupta and Jauhari, 1994). Nevertheless, the distribution pattern of CaO in the present study area goes very well with the distribution pattern of calcareous sediment shown in Banerjee, (1998).

"Excess" silica, which can be considered of biogenic origin, was calculated using the formula described by Bostrom (1976):

$$\text{SiO}_2 (\text{ex}) = \text{SiO}_{2\text{total}} - 3.38 (\text{Al}_2\text{O}_{3\text{total}}) \dots \dots \dots (5)$$

where 3.38 is the SiO₂/Al₂O₃ ratio of average deep-sea clay (Turekian and Wedephol, 1961). The calculation is based on the fact that the SiO₂/Al₂O₃ ratio in terrigenous clay and deep sea clay is more or less constant; averaging about 3.38 and whatever extra is there, is due to the biogenic silica, coming from diatoms and radiolaria. Hence, in case of siliceous and T-S sediments it is much higher (34% and 43% respectively) while in case of calcareous and red clay sediments it is nearly the same (~28.4%) (Fig 3d).

Sr is also a good productivity indicator especially in case of calcareous organisms as it can replace Ca^{+2} ions. As a result, it showed excellent correlation with Ca in siliceous-red clay transition and red clay sediments. Ba is another trace element which is known to take part in biogeochemical cycle (Schroeder et al, 1997; Agnihotri et al, 2003; Gonnee and Paytan, 2006) and showed similar distribution pattern like that of Sr. It is the essential element in barite which forms authigenically in the water column and sinks to the sediment. Ba showed highest concentration in calcareous sediment (average $\sim 3990.5\text{mg/kg}$), followed by red clay (average $\sim 3043.6\text{mg/kg}$), then siliceous ooze (average $\sim 2897.6\text{mg/kg}$) and lowest in T-S sediment (average $\sim 2134.5\text{mg/kg}$).

3.6. Trace element distribution:

Among the trace metals, V, Ni and Th showed similar distribution pattern, with highest concentrations in red clay, followed by calcareous, then siliceous and least in T-S sediment (Table 2). Pb and Nb showed highest concentrations in red clay, lowest in calcareous sediment and almost similar values in siliceous and T-S sediment (Table 2). Cu and Sr showed highest concentrations in calcareous sediment, followed by red clay, siliceous sediments and least in T-S sediment (Table 2). On the other hand, Rb and Y showed similar distribution pattern with highest concentration in red clay, followed by siliceous, calcareous and lowest in T-S sediment (Table 2). Although both Ba and Cr showed lowest concentration in T-S sediment, Ba showed highest concentration in calcareous sediment whereas, Cr exhibited highest concentration in siliceous sediment (Table 2). Zr and Sc both showed highest concentrations in red clay and lowest in calcareous sediment, but their distribution patterns were somewhat different. The second highest concentration of Zr was found in T-S sediment whereas, for Sc it was siliceous sediment (Table 2). Zn exhibited a totally different distribution pattern from the others, with highest concentration in T-S sediment, followed by siliceous, then red clay and lowest in calcareous sediment (Table 2). Out of these fourteen elements, Ba, Cr, V, Ni, Th, Rb and Y showed higher affinity towards the excess part of Fe; Pb and Sc showed more affinity towards terrigenous part of Fe, Sr and Zr showed better association with $\text{Al}_{\text{excess}}$ whereas Cu was more strongly correlated to $\text{Mn}_{\text{excess}}$ (Table 4). Zn and Nb did not show any significant relation with either terrigenous or “excess” parts of Al, Mn and Fe (Table 4).

3.7. Q-mode factor Analysis:

From the Q-mode factor analysis of the major element oxide data of the surface sediments under study, it can be seen that there are two major contributing factors accounting for 99.75% of the total variance (Table 5). Among them, Factor 1 alone accounts for 99.27% of the total variance, with the highest loading of SiO_2 . The distribution pattern of Factor 1 (Fig 4a), when plotted against station

locations, resembled the distribution pattern of $\text{SiO}_{2\text{excess}}$ (Fig 3d) with maximum concentration showing in the central part of the study area, between 11° - 13° S latitude and 75° - 77° E longitude. This area is dominantly covered by siliceous sediment of which a major fraction comes from the hard parts of the siliceous micro-organisms. Factor 2, on the other hand, accounts for only 0.48% of the total variance and shows a negative relation with CaO concentration of the surface sediment samples. Its value increases where CaO concentration decreases and vice versa. Here, the negative sign of the factors does not indicate their actual concentrations. Hence, the westernmost part of the study area, consisting mainly of calcareous sediment shows the lowest loading of Factor 2 (Fig 4b)

On the other hand, result of the Q-mode factor analysis of trace element data revealed four factors, accounting for 98.88% of the total variance together (Table 5). Out of these four factors, Factor 1 contributes 85.15% of the total variance and has the highest loading of Cu and moderate loadings of Zn and Ni. Their distribution pattern revealed maximum concentration in the siliceous sediment zone (Fig 5a). Factor 2 represents an anticorrelation with Zr and Zn concentrations. They contribute about 7.27% of the total variance and their concentration was found to be highest towards the northern and southern part of the study area (Fig 5b). Again, Factor 3 shows negative correlation with Sr and Ni concentrations. They account for about 5.08% of the total variance and shows maximum concentration in the western and south-eastern part of the study area, dominated by calcareous and red clay sediments respectively (Fig 5c). And finally Factor 4 contributes for 1.38% of the total variance and has the highest loading of Zn and a moderate loading of Sr. Their distribution pattern revealed a gradual decrease in concentration from the northern stations towards south (Fig 5d).

4. Discussion:

4.1. Geochemical characteristics of the different sediment types of CIB:

4.1.1. Calcareous sediment:

The samples from calcareous ooze zone (between 11° - 15° S latitudes and 73° - 74° E longitudes) showed high oxidizing bottom water environment with highest concentrations of CaO, Sr, Cu and Ba (Table 1b & 2). This is probably due to the upwelling of cooler water in this region (10° - 15° S latitude), enhancing surficial biological productivity and flux of biogenic materials to the seafloor (Cronan and Moorby, 1981). Although the depths of the stations in calcareous sediment zone were below the CCD, nevertheless CaO concentrations of these samples were found to be much higher than the samples from other sediment types. The reason behind this could be the proximity of this area to the Central Indian Ridge, where the rate of surface production exceeds the rate of carbonate

dissolution. So, the chances of preservation of calcareous materials are higher in this zone with respect to the other sampling sites. From Table 1b, it can be seen that, the calcareous sediment of the CIB had the highest Al/Ti ratio with corresponding high Al_{excess} and lowest Terri% values. A moderate, positive correlation is observed between Al_{excess} and Al/Ti ratio of calcareous sediments ($R = 0.67$ for $n = 5$). But most of the land derived elements like Pb, Zn, Nb, Zr, Sc, terrigenous parts of Fe and Al, alongwith $SiO_{2\text{excess}}$ were lower in concentration in calcareous sediment than in the other sediment types (Table 1b & 2).

4.1.2. Terrigenous-siliceous transition sediment:

In case of elemental abundance, the sediment of this zone has the least concentration of most of the elements except $SiO_{2\text{excess}}$, Pb, Zn, Nb, Zr and Sc (Table 1b & 2). Similar values of Al/Ti ratio to that of modern day river load and average shale composition in this sediment type indicate influence of fluvial input. Due to this, excess values of Fe, Mn and Al were lowest here with a corresponding minimum bottom water oxidizing environment. Factor analysis of trace elements also showed higher loadings of Zr and Zn in the northern part of the study area, dominated by T-S sediment. $SiO_{2\text{excess}}$ values of these samples showed a significant positive correlation with the Terri% of the samples ($R = 0.89$ for $n = 6$) indicating that excess SiO_2 , in this zone, might also come from the dissolution of land derived materials (quartz, feldspar, aluminosilicates etc.) and glass shards, besides being biogenic in nature. The very low concentration of CaO in T-S sediment is mainly due to the alterations of calcium rich minerals like feldspars, derived from the continent.

4.1.3. Siliceous sediment:

Next to the T-S sediment, the siliceous sediment samples had the highest $SiO_{2\text{excess}}$ concentrations. The volcanogenic and terrigenous components are also low here. This indicates that this area lies below the high surface productivity zone with less terrigenous as well as volcanic input than the rest of the study area. In one of the samples from this zone, negative value of Mn^* was obtained (station no. 38/195) indicating a localized sub-oxic condition. This was probably due to the diagenetic condition prevailing in these sediments. The area between 12° - 13.7° S latitude exhibits higher $SiO_{2\text{excess}}$ values and very low CaO, Ba and Sr values whereas, the area between 13.7° - 14.5° S latitude shows the opposite trend (Fig 2). The samples falling in the southern sector of siliceous zone were closer to the transition zone of the siliceous and red clay sediments with shallower water depths for which chances of preservation of calcareous hard parts are more than siliceous hard parts. This kind of topographic influence on the facies change has been mentioned by Gupta and Jauhari (1994) also. This could be the reason behind the great variation of Sr concentration in this zone from as low as

1.34mg/kg in the high productivity zone where $\text{SiO}_{2\text{excess}}$ is >40% on average, to as high as 223.4mg/kg near the transition zone of siliceous and red clay sediment where $\text{SiO}_{2\text{excess}}$ is <30% on average. The Al/Ti ratios of all the studied sediment samples from this area were very similar to the Pacific hemipelagic sediments (18 to 22).

4.1.4. Red clay:

The samples from red clay showed high oxidizing bottom water environment and highest concentrations of both the terrigenous and excess parts of Mn and Fe (Table 1b). $\text{Al}_{\text{excess}}$ and Terri% concentrations were also very high in this sediment type, alongwith the highest concentrations of V, Ni, Pb, Nb, Th, Rb, Y, Zr and Sc (Table 1b & 2). The Al/Ti ratios of all the studied sediment samples from this area were very similar to the UCC Al/Ti ratio. This area is nearer to the South-Eastern Indian Ridge and exhibited very low sedimentation rate. The finest clay particles from the land and ridge areas get deposited here. And since clay has very high surface area, it can adsorb more metals to its surface than any other size class. Hence, the concentrations of all these major and trace metals are high in this sediment type. The presence of abundant glass shards and other volcanogenic materials (pumice, palagonite, zeolite etc.) could be the possible source of both excess Al and SiO_2 .

4.2. Nature of sedimentation:

The concentration of Ti, Al, Mn and Fe increased southwards, away from the continent. Excess amounts of Al, Fe and especially Mn were found in all the studied sediment samples, which is not supported by the terrigenous source. This indicates that these three elements (Mn, Fe and Al) had a secondary supply source. A probable source of supply of these elements can be from the adjacent mid oceanic ridge rocks and basinal seamounts. Among the rock types identified in this basin presence of “ferro-basalts” are mentioned by various authors (Iyer et al, 1999; Das et al, 2012) and these rocks contain high amounts of FeO and less MgO. However, their metal content is much higher than the sediments under study and is rather closer to PAAS and upper continental crust (UCC) values. Al/Ti ratio of the sediment samples also provides signature of fluvial input upto 14°S latitude, beyond which the ratio shows value of UCC mainly, in the red clay zone. Thus, the elevated Al/Ti ratio observed in the calcareous sediments could be due to the excess Al derived from the hydrothermal emanations from the nearby mid-oceanic ridge (Thi Dieu Vu and Sohrin, 2013). Again early diagenetic enrichment due to dissolution of biogenic component can also cause enrichment of Fe and Mn in these sediments (Banerjee et al, 1991; Banerjee 1998; Wang et al, 2012). However, early diagenetic enrichment or terrestrial input cannot account for 10-25 times enrichment of Mn (with respect to PAAS value) in the surface sediments of the CIB. One of the main sources of marine

iron and manganese are the under-water volcanoes and hydrothermal vents (Bostrom and Peterson, 1966; Bonatti and Nayudu, 1965; Lynn and Bonatti, 1965; Krauskopf, 1957; Nishioka et al, 2013) and there are evidences of abundant glass shards and other volcanogenic components in the CIB sediments, which were reported to have been derived from the wide spread Toba Tuff explosion and past in situ volcanism in this basin (Sukumaran et al, 1999; Pereira et al., 2006, 2016). These could be also a potential source of both $\text{SiO}_{2\text{excess}}$ and $\text{Al}_{\text{excess}}$. Thus the main source of $\text{Mn}_{\text{excess}}$ and to some extent $\text{Fe}_{\text{excess}}$ in the surface sediments of the CIB is most probably from hydrothermal plumes and past intra-plate volcanisms.

A considerable amount of Fe and Al is contributed by aerosols in the Arabian Sea and Bay of Bengal from Arabia, Africa and Asian deserts (Kumar et al., 2010; Grand et al., 2015a; Grand et al., 2015b). The flux of these airborne particles gradually diminishes further away from the continents. For example, it has been shown by Duce and Tindale (1991) that the flux of iron is higher in the northern oceans than the southern oceans. Hence, it will be difficult to differentiate between aeolian input and fluvial input on the basis of geochemical parameters only, without any direct measurement of dust influx. However, from Table 6 it can be seen that $\text{SiO}_{2\text{excess}}$ did not show any correlation with $\text{Terri}\%$ or $\text{Al}_{\text{excess}}$, which are the parameters for detrital input in the sediment. Hence, it can be said that, most of the $\text{SiO}_{2\text{excess}}$ in the CIB sediments are biogenic in nature. This observation goes well with the factor analysis result of the major element oxides, where more than 99% of the total variance is contributed by SiO_2 alone and its distribution pattern reveals maximum concentration in the siliceous ooze zone. It should be noted here that, unlike the excess and terrigenous parts of Mn and Fe, $\text{Al}_{\text{excess}}$ and Al_{terri} showed no significant correlation (Table 4). Thus their sources might be significantly different. However, the same cannot be said for Mn and Fe as it is possible that a significant proportion of excess Mn and Fe were originally land derived but were later diagenetically remobilized in the sediment column.

4.3. Redox conditions:

To understand the redox condition in the CIB surface sediments, Mn^* and V/Cr ratio have been used. Both these parameters indicate that the CIB surface sediments were deposited under oxidized bottom water condition. The entry of cold, oxygen rich Antarctic Bottom water (AABW) into this region through the northern saddles of Ninety East Ridge is the main reason behind this (Banerjee 1998; Vineesh et al., 2009). The lowest values of both the parameters were observed in T-S sediment. The highest values of Mn^* was seen in the calcareous sediment (Tables 1b) and that of V/Cr ratio in the red clay samples. Most of the trace elements including V showed highest concentrations in the red clay sediments. The greater surface area of the clay minerals facilitates more metal adsorption than

any other grain size, for which red clay sediments had inherently more metal content than the other sediment types. This could be the reason behind the disparity between the higher values of Mn* and V/Cr ratio.

4.4. Possible source/s of metals:

The major proportion of bulk iron is terrigenous in nature which is about 60%, while the rest ~40% is excess in nature. This excess amount might have been derived from the Fe-rich ridge rocks, besides volcanogenic and other authigenic sources. From the trace metal association pattern, it was seen that the majority of the metals were associated with the excess part of Fe (Ba, Cr, V, Ni, Th, Rb and Y), while Pb and Sc showed stronger relation with Fe_{terri}. On the other hand, Cu showed strongest correlation with Mn_{excess} (Table 3). Similar metal association pattern was also observed in Sensarma et al (2016). Sr and Zr showed greater affinity towards Al_{excess} than the terrigenous part of Al. However, it has been reported by many authors that Zr might also come from aeolian source such as loess (Schnetger, 1992) and Saharan desert (Wehausen and Brumsack, 1999) in this part of the ocean. But without any direct measurement of dust influx, the extent of aeolian input could not be determined properly. Again Sr and Ba show significant, positive relation in all types of sediments (Fig 6a & b). Sr also showed good, positive regression with Ca in samples with higher Sr concentration (132-252mg/kg) in the red clay and siliceous-red clay transition zone sediments (Fig 6c). However, in case of lower Sr concentrations (0.9-2.5mg/kg), Ca showed no significant regression relation in T-S and siliceous sediments. Similar pattern was observed between Ca and Ba where the regression relation became progressively positive towards higher concentrations (Fig 6d). As was mentioned earlier, the low CaO content of siliceous and T-S sediment samples could be derived from the alterations of calcic minerals like feldspar and not from calcareous organisms. So this could be the reason of insignificant correlation of Ca with Sr and Ba. When Ca, Ba and Sr concentrations of the samples were plotted against the station depths, negative regression relations were obtained (Fig 7). Thus from the above observations it can be said that, with increasing water depth most of the hard parts of calcareous organisms get dissolved and whatever CaO is left comes from the alterations of calcic minerals. While, in shallower water depth, carbonates are preserved for which Ba and Sr showed positive relationship with Ca.

Q-mode factor analysis of the trace elements revealed highest loadings of Cu, Ni and Zn in the central part of the study area, dominated by siliceous sediment. All these trace elements are found in high concentrations in the micro-nodules, present in the bulk siliceous sediment of this area (Banerjee and Iyer, 1991). Sequential extraction study of the sediments of this area also revealed maximum association of Cu and Ni with Mn which mainly comes from the freshly precipitating,

easily reducible Mn-oxyhydroxide phase (Sensarma et al, 2016). Although, Zn was not found to be correlated to either excess or terrigenous part of Mn in the present study, its association with Mn-oxyhydroxide phases is observed elsewhere (Fernex et al, 1992; Koschinsky et al, 2003). Again, Zr and Zn were found to be higher in the northern and southern part of the study area, which are closer to landmass and south-east Indian Ridge respectively. Moreover, Zr was found to be very well correlated to Al_{excess} whose concentration increases towards the ridge. Thus, it is possible that Zr, and to some extent Zn, are contributed by the detrital fraction of the sediment. Sr and Ni, on the other hand, were found to be more in the western and south-eastern part of the study area, dominated by calcareous and red clay sediments respectively. As was mentioned earlier, Sr is a very good productivity indicator in case of calcareous sediment and shows excellent correlation with Ca in siliceous-red clay transition and red clay sediments. Hence it is natural to find higher loadings of Sr in these sediments. Ni is again known to take part in biogeochemical cycles for which it shows very good positive relation with Ca ($R = 0.88$ for $n = 35$). Similar observation was made in Sensarma et al, (2016). Thus this could be the reason of higher loading of Ni in both calcareous and red clay sediments. And lastly, Factor 4 of the trace element data shows higher loadings of Zn and to some extent Sr, whose concentrations decreases from north to south, away from the continent, thus supporting the previous observation of Zn being contributed by a detrital source. The higher concentration of Factor 4 in the western part of the study area could be due to the supply of Zn and Sr from the ridge areas and calcareous organisms respectively.

5. Conclusion:

The surface sediments of Central Indian Basin (CIB) were deposited under oxic condition due to the circulation of Antarctic Bottom water through the deeper saddles and lobes of mid-oceanic ridges surrounding the basin. However, sedimentation rate and topography of the area could create localized sub-oxic environment as was observed in few station in the siliceous sediment zone. Among the different sediment types, calcareous sediments and red clay domains showed higher oxic bottom water environment due to their shallower water depths and proximity to the ridge areas. Whereas, terrigenous-siliceous transition zone (T-S) and siliceous ooze domains are located at much higher water depth and received more continental and biogenic silica input. They showed less oxic bottom water environment and higher $SiO_{2\text{excess}}$ concentrations than calcareous and red clay sediments. Terrigenous influence on the CIB sediments could be traced to $15^{\circ}30'S$ latitude, after which it started decreasing, as indicated from the shale normalized Ti concentrations of the studied sediment samples. The terrigenous fraction was dominated by fluvial input as was ascertained from the Al/Ti ratio of the studied sediment samples.

Aluminium, iron and manganese concentrations in these sediments increased southwards, away from the continent. Al_{excess} concentration was higher in the samples nearer to the ridge areas and fracture zones (73° , $76^{\circ}30'$, $79^{\circ}E$), consisting of more calcareous and red clay sediments than in the samples farther away (T-S and siliceous sediments), indicating hydrothermal activity in those areas. Major part of iron was terrigenous in nature while its excess portion was derived from the early diagenetic enrichment in the sediment column and volcanic precursors in the basin. On the other hand, manganese concentrations in these sediments were much higher than continental and average shale values, indicating possibility of local under-water volcanism and emanations from hydrothermal vents as their source. Most of the $SiO_{2\text{excess}}$ was biogenic in origin, coming from radiolarian shells mainly, although contribution from the dissolution of glass shards and other volcanic minerals cannot be overruled. CaO concentrations of the sediments were negligible except in calcareous sediments, and Sr and Ba seem to have been associated with this phase. Thus they were mostly biogenic in nature. However, trace metals like Ni, Cr, V, Y, Rb and Th were associated mostly with Fe_{excess} , whereas Pb and Sc showed higher affinity towards Fe_{terri} . Cu, on the other hand, showed maximum association with Mn_{excess} and Zr with Al_{excess} . Thus, it can be said that the trace metals associated with Fe were mostly detrital in nature and those associated with Mn_{excess} and Al_{excess} have a volcanogenic source of supply.

Acknowledgement:

The authors are thankful to the Director, CSIR-NIO, Goa for permitting to carry out this work. Dr. S. M. Gupta is thanked for helping out with paleoceanographic studies and Mr. C. Moraes is thanked for XRF analysis. CSIR-NGRI is thanked for the ICP-MS analysis. S. Sensarma gratefully acknowledges the support of CSIR Senior Research Fellowship, India. S. Mukhopadhyay gratefully acknowledges the financial support from DST-PURSE (phase II) of Jadavpur University. It is confirmed hereby that there exists no conflict of interest among the co-authors of this manuscript. This work is a part of the Council of Scientific and Industrial Research (CSIR) supported by GAP-2175 and bears NIO contribution number XXXX.

References

- Agnihotri, R., Sarin, M.M., Somayajulu, B.L.K., Jull, A.J.T., Burr, G.S. 2003.** Late-Quaternary biogenic productivity and organic carbon deposition in the eastern Arabian Sea. *Palaeogeography, Palaeoclimatology, Palaeoecology* **197**, 43-60.
- Banakar, V.K., Parthiban, G., Pattan, J.N., Jauhari, P. 1998.** Chemistry of surface sediment along a north-south transect across the equator in the Central Indian Basin: an assessment of biogenic and detrital influences on elemental burial on the seafloor. *Chemical Geology* **147**, 217-232.

- Banerjee, R., Iyer, S.D., Dutta, P. 1991.** Buried Nodules and Associated Sediments from the Central Indian Basin. *Geo-Marine Letters* **11**, 103-107.
- Banerjee, R., Iyer, S.D. 1991.** Biogenic influence on the growth of ferromanganese micronodules in the Central Indian Basin. *Marine Geology* **97**, 413-421.
- Banerjee, R. 1998.** Mineralogical and geochemical characters of surface sediments from the Central Indian Basin. *Current Science* **75 (12)**, 1364-1371.
- Bonatti, E., Nayudu, Y.R. 1965.** The origin of manganese nodules on the ocean floor. *American Journal of Science* **263**, 17-39.
- Borole, D.V. 1993.** Late Pleistocene sedimentation: a case study of the Central Indian Ocean Basin. *Deep-Sea Research Part-I* **40 (4)**, 761-775.
- Boström, K. 1976.** Particulate and dissolved matter as sources for pelagic sediments. *Stockholm Contributions in Geology* **30 (2)**, 16-70.
- Boström, K., Peterson, M.N.A. 1966.** Precipitates from hydrothermal exhalations on the East Pacific rise. *Economic Geology* **61**, 1258-1265.
- Boyle, E.A. 1983.** Chemical accumulation variations under the Peru Current during the past 130,000 years. *Journal of Geophysical Research* **88 (C12)**, 7667-7680.
- Cronan, D.S., Moorby, S.A. 1981.** Manganese nodules and other ferromanganese oxide deposits from the Indian Ocean. *Journal of the Geological Society of London* **138**, 527-539.
- Das, A., Sujith, P. P., Mourya, B.S., Biche, S.U., LokaBharathi, P. A. 2011.** Chemosynthetic activity prevails in deep-sea sediments of the Central Indian Basin. *Extremophiles* **15**, 177–189. DOI 10.1007/s00792-010-0346-z.
- Das, P., Iyer, S.D., Hazra, S. 2012.** Petrologic Characteristics and Genesis of the Central Indian Ocean Basin Basalts. *Acta Geologica Sinica (English edition)* **86 (5)**, 1154-1170.
- Dill, H., Teshner, M., Wehner, H. 1988.** Petrography, inorganic and organic geochemistry of Lower Permian Carboniferous fan sequences (“Brandschiefer Series”) FRG: constraints to their paleogeography and assessment of their source rock potential. *Chemical Geology* **67**, 307– 325.
- Duce, R.A., Tindale, N.W. 1991.** Atmospheric transport of iron and its deposition in the ocean. *Limnology and Oceanography* **36**, 1715–1726.
- Fernex, F., Fevrier, G., Benaim, J., Arnoux, A. 1992.** Copper, lead and zinc trapping in Mediterranean deep-sea sediments: probable coprecipitation with Mn and Fe. *Chemical Geology* **98**, 293-306.
- Gonneea, M.E., Paytan, A. 2006.** Phase associations of barium in marine sediments. *Marine Chemistry* **100**, 124-135.
- Gordeev, V.V., Lisitzyn, A. P. 1979.** Microelements. *Chemistry of the Ocean*: Moscow (Nauka).

Grand, M.M., Measures, C.I., Hatta, M., Hiscock, W.T., Buck, C.S., Landing, W.M. 2015a. Dust deposition in the eastern Indian Ocean: The ocean perspective from Antarctica to the Bay of Bengal. *Global Biogeochemical Cycles* **29**, 357–374, DOI:10.1002/2014GB004898.

Grand, M.M., Measures, C.I., Hatta, Morton, P.L., Barrett, P., Milne, A., Resing, J.A., Landing, W.M., 2015b. The impact of circulation and dust deposition in controlling the distributions of dissolved Fe and Al in the south Indian subtropical gyre. *Marine Chemistry* **176**, 110–125.

Gupta, S.M., Jauhari, P. 1994. Radiolarian abundance and geochemistry of the surface-sediments from the Central Indian Basin: Inferences to Antarctic bottom water current. *Current Science* **66 (9)**, 659-663.

Iyer, S.D., Mukhopadhyay, R., Popko, D.C. 1999. Ferrobasalts from the Central Indian Ocean Basin. *Geo-Marine Letters* **18**, 297-304.

Jones, B., Manning, D.A.C. 1994. Composition of geochemical indices used for the interpretation of paleoredox conditions in ancient mudstones. *Chemical Geology* **111**, 111 – 129.

Juggins, S. 2003. C2 user guide, Software for ecological and paleoecological data analysis and visualization, University of Newcastle, Newcastle upon Tyne, UK, p. 69.

Kamesh Raju, K.A. 1993. Magnetic lineations, fracture zones and seamounts in the Central Indian Basin. *Marine Geology*, **109**, 195-201.

Kamesh Raju, K.A., Ramprasad, T., Kodagali, V.N., Nair, R.R. 1993. Multibeam bathymetric, gravity and magnetic studies over 79⁰E fracture zone, Central Indian Basin. *Journal of Geophysical Research* **98 (B6)**, 9605-9618.

Kodagali, V.N., Kamesh Raju, K.A., Ramprasad, T., George, P., Jaishankar, S. 1992. Detailed bathymetric surveys in the Central Indian Basin. *International Hydrographic Review, Monaco*, **69**, 143-150.

Kolla, V., Sullivan, L., Streeter, S.S., Langseth, M.G. 1976. Spreading of Antarctic bottom water and its effects on the floor of the Indian Ocean inferred from bottom-water potential temperature, turbidity and sea floor photography. *Marine Geology* **21**, 171-189.

Koschinsky, A., Winkler, A., Fritsche, U. 2003. Importance of different types of marine particles for the scavenging of heavy metals in the deep-sea bottom water. *Applied Geochemistry* **18**, 693–710.

Krauskopf, K.B. 1957. Separation of manganese from iron in sedimentary processes. *Geochimica et Cosmochimica Acta* **12 (1-2)**, 61-84.

Kumar, A., Sarin, M.M., Srinivas, B. 2010. Aerosol iron solubility over Bay of Bengal: Role of anthropogenic sources and chemical processing. *Marine Chemistry* **121**, 167–175.

Lynn, D.C., Bonatti, E. 1965. Mobility of manganese in diagenesis of deep sea sediments. *Marine Geology* **3**, 457-474.

Machhour, L., Philip, J., Oudin, J.L. 1994. Formation of laminite deposits in anaerobic-dysaerobic marine environments. *Marine Geology* **117**, 287-302.

- Mukhopadhyay, R., Ghosh, A.K., Iyer, S.D. 2008.** The Indian Ocean Nodule Field: Geology and Resource Potential. (Handbook of Exploration and Environmental Geochemistry, 10; Hale, M.: ed.). Elsevier, Amsterdam, The Netherlands.
- Murdmaa, I., Gordeev, V., Kuzmina, T., Turanskaya, N., Mikhailov, M. 1980.** Geochemistry of the Japan Trench sediments recovered on Deep Sea Drilling Project Legs 56 and 57, in *Initial Report of Deep Sea Drilling Project* **56-57**, 1213-1232.
- Murray, R.W., Leinen, M. 1996.** Scavenged excess aluminium and its relationship to bulk titanium in biogenic sediment from the central equatorial Pacific Ocean. *Geochimica et Cosmochimica Acta* **60**, 3869-3878.
- Nath, B.N., Rao, V.P., Becker, K.P. 1989.** Geochemical evidence of terrigenous influence in deep-sea sediments upto 8°S in the Central Indian Basin. *Marine Geology* **87**, 301-313.
- Nishioka, J., Obata, H., Tsumune, D. 2013.** Evidence of an extensive spread of hydrothermal dissolved iron in the Indian Ocean. *Earth and Planetary Science Letters* **361**, 26–33.
- Parsons, T.R., Takahashi, M., Hargrave, B. 1977.** Biological Oceanographic Processes. Pergamon Press, Oxford, UK 2nd ed, 332pp.
- Pattan, J.N., Guptha, S.M., Mudholkar, A.V., Parthiban, G. 1992.** Biogenic silica in space and time in sediments of Central Indian Ocean. *Indian Journal of Marine Sciences* **21**, 116-120.
- Pattan, J.N., Masuzawa, T., Borol, D.V., Parthiban, G., Jauhari, P., Yamamoto, M. 2005.** Biological productivity, terrigenous influence and noncrustal elements supply to the Central Indian Ocean Basin: Paleoceanography during the past ~1 Ma. *Journal of Earth System Science* **114 (1)**, 63-74.
- Pereira, M.B.L.M., Nath, B.N., Borole, D.V., Gupta, S.M. 2006.** Nature, source and composition of volcanic ash in sediments from a fracture zone trace of Rodriguez Triple Junction in the Central Indian Basin. *Marine Geology* **229**, 79–90.
- Pereira, M.B.L.M., Nath, B.N., Borole, D.V., Parthiban, G., Jijin, R., Khedekar, V.D. 2016.** Multiple ash layers in late Quaternary sediments from the Central Indian Basin. *Journal of Volcanology and Geothermal Research* **316**, 85-100.
- Rao, V.P., Nath, B.N. 1988.** Nature, Distribution and Origin of Clay Minerals in Grain Size Fractions of Sediments from Manganese Nodule Field, Central Indian Ocean Basin. *Indian Journal of Marine Sciences* **17**, 202-207.
- Sabine, C.L., Key, R.M., Feely, R.A., Greeley, D. 2002.** Inorganic carbon in the Indian Ocean: Distribution and dissolution processes. *Global Biogeochemical Cycles* **16**, 15-11-15-18.
- Schroeder, J.O., Murray, R.W., Leinen, M., Pflaum, R.C., Janecek, T.R. 1997.** Barium in equatorial Pacific carbonate sediment: Terrigenous, oxide, and biogenic associations. *Paleoceanography* **12 (1)**, 125-146.
- Schnetger, B. 1992.** Chemical composition of loess from a local and worldwide view. *Neues Jahrbuch der Mineralogie* **1**, 29-47.

- Sensarma, S., Chakraborty, P., Banerjee, R., Mukhopadhyay, S. 2016.** Geochemical fractionation of Ni, Cu and Pb in the deep sea sediments from the Central Indian Ocean Basin: An insight into the mechanism of metal enrichment in sediment. *Chemie der Erde Geochemistry* **76**, 39–48.
- Sukumaran, N.P., Banerjee, R., Borole, D.V., Gupta, S.M. 1999.** Some aspects of volcanic ash layers in the Central Indian Basin. *Geo-Marine Letters* **18**, 203-208.
- Taylor, S.R., McLennan, S.M. 1985.** The continental crust: its composition and evolution. *Blackwell Scientific Publication, Oxford*, 312 pp.
- Thi Dieu Vu, H., Sohrin, Y. 2013.** Diverse stoichiometry of dissolved trace metals in the Indian Ocean. *Scientific Reports* **3**, 1745. DOI: 10.1038/srep01745.
- Turekian, K.K., Wedepohl, K.H. 1961.** Distribution of the Elements in some major units of the Earth's crust. *Geological Society of America Bulletin* **72**, 175-192.
- Valsangkar, A.B., Ambre, N.V. 2000.** Distribution of Grain Size and Clay Minerals in Sediments from the INDEX Area, Central Indian Basin. *Marine Georesources & Geotechnology* **18**, 189-199.
- Valsangkar, A.B. 2011.** Spatial Distribution and Longitudinal Variation of Clay Minerals in the Central Indian Basin. *Acta Geologica Sinica (English edition)* **85 (4)**, 814-825.
- Vineesh, T.C., Nagender Nath, B., Banerjee, R., Jaisankar, S., Lekshmi, V. 2009.** Manganese nodule morphology as indicators for oceanic processes in the Central Indian Basin. *International Geology Review* **51 (1)**, 27–44
- Wang, X., Gan, L., Wiens, M., Schloßmacher, U., Schröder, H.C., Müller, W.E.G. 2012.** Distribution of Microfossils within Polymetallic Nodules: Biogenic Clusters within Manganese Layers. *Marine Biotechnology* **14**, 96–105. DOI: 10.1007/s10126-011-9393-4.
- Wedepohl, K.H. 1978.** Handbook of Geochemistry 2, *Springer-Verlag, Berlin, Heidelberg, New York*.
- Wehausen, R., Brumsack, H.J. 1999.** Cyclic variations in the chemical composition of eastern Mediterranean Pliocene sediments: a key for understanding sapropel formation. *Marine Geology* **153**, 161-176.

List of Tables:

Table 1a: Major element oxide data (measured in XRF) of the CIB surface samples under study with locations and sediment types.

Station	Lat°S	Long°E	Depth (m)	Sedi type	SiO ₂	TiO ₂	Al ₂ O ₃	Fe ₂ O ₃	MnO	CaO	MgO	Na ₂ O	K ₂ O	P ₂ O ₅	LOI%
38/2	8.50	78.00	5438	Terri-Sili	61.99	0.32	9.81	3.88	0.07	0.64	1.35	1.55	2.47	0.08	17.84
38/189	11.51	75.94	5433	"	70.11	0.41	7.60	3.36	0.23	0.30	0.91	1.14	1.26	0.06	14.62
38/188	11.56	75.88	5433	"	67.43	0.38	7.90	3.86	0.29	0.34	1.20	1.67	1.38	0.07	15.48
38/185	11.63	75.81	5430	"	69.57	0.38	7.52	3.67	0.29	0.30	1.09	1.23	1.24	0.05	14.66
38/187	11.67	75.87	5433	"	69.70	0.37	7.49	3.78	0.57	0.30	1.05	0.90	1.23	0.06	14.55
38/186	11.74	75.81	5433	"	69.99	0.38	8.08	4.25	0.55	0.32	1.22	0.70	1.37	0.05	13.09
6/17G	11.50	73.26	5390	Calcareous	55.52	0.21	8.42	3.20	1.16	28.32	2.07	0.68	1.34	0.26	-1.18
6/16A	11.75	73.25	5360	"	67.93	0.36	10.35	4.46	1.04	10.57	2.71	0.84	1.74	0.26	-0.26
6/15D	12.06	73.26	5350	"	60.00	0.26	9.22	3.72	1.29	21.53	2.33	0.68	1.49	0.26	-0.78
6/11C	14.26	73.01	5290	"	67.91	0.42	12.02	5.66	1.33	5.60	2.87	1.92	2.02	0.34	-0.09
7/28E	14.75	73.51	4896	"	65.91	0.40	11.84	5.19	1.37	9.41	2.95	0.80	1.80	0.28	0.05
38/192	12.08	75.80	5430	Siliceous	54.27	0.30	8.29	3.82	0.83	0.71	1.90	5.91	1.65	0.15	22.17
38/191	12.13	75.80	5430	"	70.58	0.33	7.77	3.44	0.09	0.35	0.99	1.50	1.55	0.04	13.36
38/195	12.18	75.87	5433	"	70.97	0.32	7.14	3.33	0.05	0.32	0.98	1.60	1.37	0.05	13.87
38/196	12.19	75.76	5433	"	69.01	0.37	7.48	3.82	0.61	0.32	1.10	1.21	1.20	0.07	14.81
38/197	12.30	75.76	5433	"	53.93	0.29	8.19	3.75	0.79	0.69	1.85	5.97	1.67	0.14	22.73
38/194	12.31	75.87	5433	"	70.81	0.37	7.45	4.08	0.69	0.28	1.14	0.59	1.20	0.05	13.34
38/193	12.37	75.80	5430	"	68.72	0.37	7.67	4.22	1.10	0.29	1.15	0.62	1.25	0.07	14.54
38/199	12.38	75.57	5430	"	69.59	0.42	8.01	4.35	0.35	0.27	1.17	0.55	1.23	0.06	14.00
38/198	12.43	75.62	5433	"	52.44	0.28	7.91	3.66	0.73	0.68	1.96	7.10	1.62	0.15	23.47
38/205	12.51	75.18	5330	"	67.57	0.40	7.97	4.68	0.77	0.29	1.33	0.54	1.24	0.07	15.14
38/201	12.56	75.48	5433	"	68.06	0.38	8.25	4.64	0.79	0.31	1.15	0.71	1.44	0.09	14.18
38/204	12.56	75.25	5320	"	71.21	0.38	7.43	4.12	0.44	0.28	1.11	0.59	1.16	0.06	13.22
38/203	12.56	75.38	5385	"	67.60	0.40	7.82	3.82	0.42	0.33	1.04	1.42	1.30	0.09	15.76
38/206	12.57	75.13	5330	"	70.03	0.38	7.41	3.82	0.65	0.29	1.06	0.85	1.23	0.06	14.22
38/3	12.58	75.26	5320	"	46.55	0.29	7.54	3.86	0.62	0.72	1.91	7.01	1.61	0.12	29.77
38/202	12.63	75.44	5433	"	69.18	0.38	7.82	4.41	0.74	0.29	1.22	0.61	1.27	0.06	14.02
6/13C	13.49	73.48	5170	"	70.59	0.40	11.32	5.07	1.25	5.49	2.84	0.81	1.87	0.25	0.11
6/14C	13.51	73.76	5260	"	72.18	0.42	11.46	5.20	1.08	3.33	2.87	0.90	1.95	0.26	0.35
6/2F	13.73	74.26	5230	"	71.63	0.48	12.35	5.87	1.08	0.97	2.74	2.70	2.12	0.30	-0.24
6/2E	13.73	74.26	5244	"	71.34	0.50	12.88	6.28	0.98	0.91	2.89	1.61	2.05	0.29	0.27
6/12B	13.75	73.50	5240	"	71.07	0.44	11.88	5.54	1.05	2.51	2.96	1.97	2.07	0.30	0.21
38/4	14.00	75.00	4935	"	42.72	0.26	7.11	3.37	0.61	0.98	1.95	7.53	1.68	0.19	33.60
8/28B	14.00	78.25	4927	"	72.95	0.43	11.76	4.95	0.69	0.79	2.20	2.47	1.93	0.18	1.65
6/7A	14.00	74.25	5275	"	74.71	0.41	11.72	4.99	0.86	1.02	2.40	1.48	2.20	0.32	-0.11
6/8C	14.00	73.75	5300	"	69.22	0.47	13.07	6.03	1.10	1.25	2.69	1.99	2.23	0.43	1.52
6/7D	14.00	74.24	5275	"	65.22	0.56	14.84	8.65	1.54	1.45	3.18	1.49	2.55	0.60	-0.08
6/3E	14.24	74.74	5175	"	72.01	0.46	12.72	5.65	1.19	1.19	2.56	1.41	2.28	0.34	0.19
6/3D	14.25	74.74	5163	"	72.31	0.46	12.71	5.60	1.13	1.07	2.61	2.21	2.29	0.34	-0.73
8/27C	14.25	78.25	4911	"	72.65	0.44	12.07	5.11	0.79	0.85	2.30	2.32	1.97	0.20	1.30

*LOI%: Loss in ignition due to heating the sample to ultra high temperature in fusion bead method.

Station	Lat°S	Long°E	Depth (m)	Sedi type	SiO ₂	TiO ₂	Al ₂ O ₃	Fe ₂ O ₃	MnO	CaO	MgO	Na ₂ O	K ₂ O	P ₂ O ₅	LOI%
6/6B	14.26	74.24	5225	"	67.78	0.53	14.60	6.56	1.07	1.23	3.39	1.41	2.21	0.43	0.79
6/4G	14.49	74.72	5180	"	74.49	0.44	11.84	5.18	0.97	1.03	2.50	1.29	2.06	0.24	-0.04
8/10E	14.49	76.95	5315	"	74.94	0.41	11.03	4.82	0.71	0.75	2.26	1.42	1.90	0.17	1.59
6/10E	14.49	73.75	5221	"	69.34	0.42	12.16	5.34	1.17	5.34	2.84	0.99	2.04	0.39	-0.03
8/10D	14.49	76.97	5315	"	75.19	0.45	11.57	4.90	0.77	0.85	2.47	1.41	1.84	0.17	0.38
8/20	14.50	77.74	4657	"	73.49	0.46	12.80	5.28	0.92	0.96	2.47	1.69	2.21	0.23	-0.51
6/4C	14.50	74.74	5180	"	70.83	0.49	13.09	5.99	1.19	1.18	2.65	1.37	2.24	0.35	0.62
6/5A	14.50	74.24	5200	"	72.05	0.47	12.76	5.66	1.10	1.21	2.58	1.44	2.27	0.37	0.09
8/25B	14.51	77.99	4640	"	73.78	0.42	11.69	5.00	0.82	0.76	2.28	2.80	2.11	0.19	0.15
8/18D	14.74	77.47	5120	Red clay	74.13	0.42	11.67	4.78	0.75	0.84	2.17	2.70	2.15	0.20	0.19
8/3B	14.75	76.48	5570	"	69.30	0.46	12.30	5.80	1.07	0.90	2.36	3.40	2.30	0.25	1.86
8/11D	14.75	77.18	5198	"	73.41	0.43	11.75	5.01	0.87	0.84	2.26	2.59	2.06	0.21	0.57
8/9C	14.76	76.98	5431	"	70.46	0.48	12.55	5.83	1.01	0.84	2.37	3.04	2.10	0.23	1.09
8/21B	14.76	77.72	5206	"	73.59	0.43	11.93	5.10	0.91	0.83	2.28	2.78	2.10	0.22	-0.17
8/9D	14.76	76.97	5631	"	74.56	0.44	12.15	5.12	0.87	0.84	2.42	1.59	2.11	0.20	-0.30
8/24A	14.76	77.99	5110	"	72.88	0.46	12.85	5.23	0.99	1.04	2.40	1.74	2.34	0.27	-0.20
8/5F	14.76	76.72	5211	"	73.16	0.43	11.97	4.98	0.69	0.86	2.24	2.08	2.10	0.21	1.28
8/23D	15.00	77.97	5110	"	70.61	0.51	13.52	5.86	1.09	1.03	2.46	2.17	2.30	0.29	0.16
8/12G	15.00	77.21	5200	"	70.58	0.47	12.83	5.70	1.07	1.00	2.47	3.32	2.35	0.31	-0.10
8/6E	15.02	76.70	4922	"	68.18	0.49	13.20	6.18	1.29	1.73	2.70	1.93	2.32	0.46	1.52
8/16A	15.25	77.49	5118	"	67.87	0.55	14.03	6.64	1.29	1.22	2.78	1.44	2.34	0.42	1.42
8/17B	15.00	77.43	5194	"	71.53	0.48	12.75	5.63	1.05	1.00	2.46	1.91	2.17	0.30	0.72
8/17E	15.01	77.49	5129	"	72.17	0.48	12.69	5.42	0.87	1.02	2.49	1.43	2.00	0.25	1.18
8/22C	15.01	77.75	5073	"	69.26	0.47	12.93	5.74	1.13	1.02	2.36	2.06	1.53	0.30	3.20
8/14C	15.50	77.22	5135	"	69.52	0.47	12.61	5.72	1.07	0.93	2.33	2.42	1.97	0.25	2.71
8/15G	15.50	77.45	5052	"	67.70	0.55	13.80	6.57	1.25	1.16	2.60	1.84	2.25	0.38	1.90
8/14G	15.50	77.21	5143	"	70.69	0.47	12.72	5.71	1.23	1.05	2.47	1.83	2.30	0.33	1.20
8/13C	15.75	77.24	5100	"	73.08	0.44	11.82	5.14	0.90	0.79	2.33	1.69	1.94	0.23	1.64
38/5	17.05	74.04	4850	"	38.91	0.42	9.96	5.58	1.24	1.32	2.31	6.14	2.94	0.35	30.83
				Mean	68.24	0.42	10.75	4.95	0.88	2.02	2.13	2.02	1.87	0.22	
				Min	38.91	0.21	7.11	3.20	0.05	0.27	0.91	0.54	1.16	0.04	
				Max	75.19	0.56	14.84	8.65	1.54	28.32	3.39	7.53	2.94	0.60	

Table 1b: The important geochemical parameters of the samples used here, based on their major element concentrations alongwith the sediment types.

Sr. No.	Station	Sedi type	Mn*	Mn (ex)	Al (ex)	SiO ₂ (ex)	Fe (ex)	Terri %	Al/Ti
1	38/2	Terri-sili	2.71	0.03	1.99	28.84	1.10	31.97	27.04
2	38/189	"	0.62	0.14	-0.02	44.42	0.32	40.46	16.58
3	38/188	"	0.67	0.19	0.39	40.72	0.80	37.96	18.36
4	38/185	"	0.69	0.19	0.19	44.17	0.67	37.86	17.51
5	38/187	"	0.97	0.41	0.30	44.40	0.81	36.66	18.01
6	38/186	"	0.90	0.39	0.45	42.69	1.06	38.26	18.62
7	6/17G	Calcareous	1.35	0.88	2.36	27.06	1.18	20.98	35.41
8	6/16A	"	1.16	0.77	1.88	32.95	1.30	35.96	25.39
9	6/15D	"	1.33	0.98	2.28	28.84	1.29	25.97	31.31
10	6/11C	"	1.16	0.99	2.17	27.28	1.84	41.96	25.27
11	7/28E	"	1.54	2.25	2.27	25.89	1.61	39.96	26.14
12	38/192	Siliceous	1.13	0.62	1.44	26.26	1.20	29.47	24.80
13	38/191	"	0.21	0.04	0.86	44.33	0.78	32.57	21.04
14	38/195	"	-0.08	0.01	0.56	46.83	0.72	32.17	19.59
15	38/196	"	0.99	0.44	0.23	43.72	0.81	37.36	17.67
16	38/197	"	1.11	0.59	1.46	26.24	1.19	28.77	25.11
17	38/194	"	1.02	0.50	0.26	45.63	1.01	36.86	17.82
18	38/193	"	1.20	0.82	0.39	42.81	1.12	36.66	18.45
19	38/199	"	0.70	0.24	0.06	42.51	0.95	41.86	16.88
20	38/198	"	1.09	0.54	1.42	25.71	1.18	27.67	25.20
21	38/205	"	1.00	0.56	0.27	40.63	1.30	39.46	17.82
22	38/201	"	1.02	0.58	0.53	40.16	1.32	38.36	18.98
23	38/204	"	0.82	0.31	0.13	46.11	0.98	38.06	17.21
24	38/203	"	0.83	0.29	0.15	41.18	0.68	39.86	17.30
25	38/206	"	1.02	0.47	0.17	44.98	0.80	37.56	17.41
26	38/3	"	1.18	0.93	2.59	32.33	1.55	39.96	24.99
27	38/202	"	2.52	0.45	1.09	21.05	1.24	28.98	22.95
28	6/13C	"	1.01	0.54	0.36	42.74	1.20	37.76	18.27
29	6/14C	"	1.11	0.80	1.87	33.45	1.54	41.96	24.09
30	6/2F	"	1.05	0.80	1.74	29.89	1.71	47.95	22.72
31	6/2E	"	0.98	0.72	1.82	27.81	1.89	49.95	22.75
32	6/12B	"	1.07	0.78	1.89	30.92	1.68	43.96	23.84
33	38/4	"	2.47	0.45	1.16	18.70	1.04	25.98	24.12
34	8/28B	"	0.93	0.50	1.93	33.20	1.31	42.96	24.15
35	6/7A	"	1.03	0.63	2.11	35.10	1.44	40.96	25.24
36	6/8C	"	1.05	0.81	2.22	25.04	1.87	46.95	24.56
37	6/7D	"	1.04	1.15	2.26	15.06	3.25	55.94	23.40
38	6/3E	"	1.11	0.88	2.14	29.02	1.65	45.95	24.42
39	6/3D	"	1.09	0.84	2.13	29.35	1.62	45.95	24.40
40	8/27C	"	0.98	0.57	1.99	31.85	1.38	43.96	24.22

Sr. No.	Station	Sedi type	Mn*	Mn (ex)	Al (ex)	SiO ₂ (ex)	Fe (ex)	Terri %	Al/Ti
41	6/6B	Siliceous	1.00	0.78	2.44	18.43	1.94	52.95	24.33
43	8/10E	"	0.96	0.52	1.74	37.66	1.32	40.96	23.76
44	6/10E	"	1.13	0.87	2.87	28.24	1.64	41.96	25.57
45	8/10D	"	0.99	0.56	1.63	36.08	1.18	44.96	22.70
46	8/20	"	1.03	0.67	2.18	30.23	1.40	45.95	24.57
47	6/4C	"	1.09	0.88	2.04	26.59	1.74	48.95	23.59
48	6/5A	"	1.08	0.81	2.06	28.92	1.61	46.95	23.97
49	8/25B	"	1.00	0.60	1.98	34.27	1.22	41.96	24.58
50	8/18D	Red clay	1.45	1.65	2.02	34.69	1.39	41.96	24.54
51	8/3B	"	1.40	1.79	2.04	27.73	1.36	45.95	23.61
52	8/11D	"	1.44	1.71	2.21	33.70	1.33	42.96	24.13
53	8/9C	"	1.40	1.79	2.10	28.04	1.61	47.95	23.09
54	8/21B	"	1.04	0.67	2.09	33.27	1.85	42.96	24.50
55	8/9D	"	1.02	0.64	1.93	33.49	1.86	43.96	24.38
56	8/24A	"	1.07	0.73	1.92	29.45	1.73	45.95	24.67
57	8/5F	"	1.44	1.70	1.93	32.70	1.33	42.96	24.58
58	8/23D	"	1.41	1.86	1.85	24.91	1.65	50.95	23.41
59	8/12G	"	1.06	0.79	2.04	27.21	1.31	46.95	24.11
60	8/6E	"	1.11	0.96	2.06	23.56	1.52	48.95	23.79
61	8/16A	"	1.08	0.95	1.96	20.45	1.51	54.95	22.53
62	8/17B	"	1.43	1.86	1.92	28.44	1.37	47.95	23.46
63	8/17E	"	1.45	1.89	2.15	29.28	1.64	47.95	23.35
64	8/22C	"	1.40	1.79	1.98	25.56	1.63	46.95	24.29
65	8/14C	"	1.40	1.76	1.81	26.90	1.82	46.95	23.69
66	8/15G	"	1.39	1.97	2.04	21.06	1.62	54.95	22.16
67	8/14G	"	1.12	0.91	1.86	27.70	1.37	46.95	23.90
68	8/13C	"	1.45	1.77	1.07	33.13	1.77	43.96	23.72
69	38/5	"	2.38	0.93	1.98	5.24	1.22	42.06	23.72
		Mean	1.16	0.85	1.55	31.90	1.37	41.55	22.92
		Min	-0.08	0.01	-0.02	5.24	0.32	20.98	16.58
		Max	2.71	2.25	2.87	46.83	3.25	55.94	35.41

Table 2: Trace element data of 35 selected sediment samples (measured in ICP-MS), representing all broad sediment types (all data in mg/kg).

Sr. No.	Station	Sedi type	Ba	Cr	V	Ni	Cu	Zn	Pb
1	38/2	Terri-Sili	1651.0	46.5	43.70	41.10	99.50	304.7	114.5
2	38/189	“	2048.1	26.5	28.50	48.40	63.50	64.80	20.90
3	38/188	“	2141.4	41.7	61.40	116.4	205.5	106.1	40.20
4	38/185	“	2263.1	41.6	60.30	132.9	218.0	210.2	38.30
5	38/187	“	2455.1	46.2	67.10	156.2	267.3	185.0	28.10
6	38/186	“	2870.5	53.4	75.50	128.2	224.5	126.0	35.20
7	38/192	Siliceous	2426.7	37.2	64.60	128.9	249.8	100.7	26.80
8	38/191	“	2818.1	42.6	58.50	72.80	143.7	114.0	32.30
9	38/195	“	2997.0	56.3	62.50	61.50	136.7	131.8	30.10
10	38/196	“	2572.6	45.2	70.20	154.7	283.8	152.4	31.40
11	38/197	“	2734.1	48.2	73.50	155.0	299.9	170.2	38.90
12	38/194	“	2527.8	52.4	67.70	145.9	266.5	119.2	29.90
13	38/193	“	2969.8	51.9	81.50	297.2	532.2	157.7	38.80
14	38/199	“	2724.1	73.8	82.50	135.6	254.4	132.4	30.40
15	38/198	“	3213.2	78.9	66.60	157.1	283.2	136.2	29.40
16	38/205	“	2846.0	44.6	64.70	130.4	230.7	128.0	28.00
17	38/201	“	2536.3	42.1	70.20	142.6	269.2	117.2	30.50
18	38/204	“	3262.8	60.7	87.30	163.2	284.3	112.0	32.40
19	38/203	“	1872.9	54.8	48.10	110.6	178.4	190.6	27.20
20	38/206	“	2560.3	36.1	66.40	162.3	287.7	119.6	30.70
21	38/3	“	2134.0	4.20	43.30	100.9	174.3	151.1	24.30
22	38/202	“	2841.0	45.6	74.30	158.6	296.9	132.5	31.80
23	6/2F	“	3151.6	75.2	123.6	433.8	438.7	153.9	40.60
24	38/4	“	817.9	19.2	48.70	105.0	181.6	534.6	260.2
25	6/7A	“	3428.2	67.9	124.2	343.1	361.5	145.5	36.80
26	6/8C	“	3266.6	69.3	136.1	452.1	463.8	155.5	43.20
27	6/3D	“	3354.6	71.7	131.8	452.2	429.6	152.4	45.30
28	6/6B	“	3913.8	75.6	140.5	407.6	402.8	153.1	43.90
29	6/4G	“	4046.5	77.8	149.0	466.0	432.6	167.2	42.50
30	8/10E	“	3781.0	59.7	111.7	274.7	292.1	125.4	34.70
31	6/5A	“	3546.4	73.6	140.3	440.8	437.4	151.9	47.80
32	8/12G	Red clay	3273.8	66.7	134.1	419.3	387.4	145.1	47.20
33	38/5	“	2435.0	36.5	69.70	287.1	242.9	141.0	186.6
34	6/17G	Calcareous	2497.0	36.1	58.60	197.7	248.7	76.30	15.40
35	6/11C	“	4883.6	64.8	130.3	376.4	413.5	138.9	38.30
		Mean	2824.6	52.13	83.34	215.9	285.2	154.4	47.22
		Min	817.90	4.20	28.50	41.10	63.50	64.80	15.40
		Max	4883.6	78.90	149.0	466.0	532.2	534.6	260.2

Sr. No.	Station	Sedi type	Th	Sr	Rb	Y	Zr	Nb	Sc	V/Cr
1	38/2	Terri-Sili	18.9	132.3	118.8	30.60	502.4	10.2	10.8	0.94
2	38/189	“	7.40	1.00	44.00	16.10	13.60	2.60	8.10	1.08
3	38/188	“	12.0	1.70	54.30	42.30	47.00	5.70	14.7	1.47
4	38/185	“	11.3	1.70	52.20	41.10	33.20	4.90	14.9	1.45
5	38/187	“	8.10	1.80	55.80	51.00	22.10	4.90	16.6	1.45
6	38/186	“	9.50	2.00	69.40	51.90	29.60	6.20	18.7	1.41
7	38/192	Siliceous	10.9	1.70	55.00	48.30	28.60	5.30	15.9	1.74
8	38/191	“	12.8	1.80	76.70	44.60	24.10	6.00	15.7	1.37
9	38/195	“	10.2	1.70	67.20	38.60	28.40	5.60	16.6	1.11
10	38/196	“	10.5	1.80	57.20	49.00	20.50	5.00	17.6	1.55
11	38/197	“	11.6	1.90	65.50	55.00	21.90	6.10	18.3	1.52
12	38/194	“	11.6	1.80	57.10	49.30	29.80	5.50	17.0	1.29
13	38/193	“	17.8	2.20	69.00	63.90	81.60	6.70	18.8	1.57
14	38/199	“	15.1	2.00	67.40	56.50	48.40	5.30	20.5	1.12
15	38/198	“	10.7	1.90	58.50	53.40	30.20	4.70	16.9	0.85
16	38/205	“	9.90	2.50	53.20	58.60	24.40	5.00	15.8	1.45
17	38/201	“	11.1	1.80	68.80	58.60	18.20	5.10	17.0	1.67
18	38/204	“	13.6	2.20	68.90	62.60	25.80	6.10	21.4	1.44
19	38/203	“	8.30	1.30	42.00	41.60	19.90	3.90	12.6	0.88
20	38/206	“	11.4	1.90	57.80	55.50	35.30	4.80	15.4	1.84
21	38/3	“	8.30	160.2	39.60	34.10	406.8	4.60	11.8	10.26
22	38/202	“	13.1	2.00	65.50	60.20	26.00	5.80	18.4	1.63
23	6/2F	“	21.2	197.8	97.10	72.70	114.1	4.20	36.5	1.64
24	38/4	“	13.2	148.8	52.50	54.40	410.5	6.00	14.2	2.54
25	6/7A	“	25.4	195.7	97.30	84.00	118.0	5.10	34.1	1.83
26	6/8C	“	29.3	213.9	102.8	124.7	130.2	5.30	39.6	1.96
27	6/3D	“	22.5	211.0	97.60	85.80	123.6	4.70	44.2	1.84
28	6/6B	“	25.1	222.4	108.4	93.60	130.0	5.30	41.1	1.86
29	6/4G	“	22.6	223.0	96.40	73.80	120.5	4.20	38.3	1.92
30	8/10E	“	17.8	189.6	82.90	47.10	108.6	3.40	35.7	1.87
31	6/5A	“	26.0	223.4	103.3	101.9	130.3	5.10	40.1	1.91
32	8/12G	Red clay	22.3	209.7	98.80	76.50	124.7	5.20	43.4	2.01
33	38/5	“	17.5	251.9	70.30	125.0	783.1	9.20	20.0	1.91
34	6/17G	Calcareous	12.6	694.6	47.90	41.30	45.50	-	-	1.62
35	6/11C	“	20.2	366.3	84.30	79.80	108.6	3.50	13.7	2.01
		Mean	15.14	105.1	71.53	60.67	113.3	5.33	22.19	1.83
		Min	7.40	1.00	39.60	16.10	13.60	2.60	8.10	0.85
		Max	29.30	694.6	118.8	125.0	783.1	10.20	44.20	10.26

Table 3: The recovery of the major element oxides and trace elements (in % of reported values) alongwith the relative standard deviation (RSD) of the certified reference materials (CRM) used in the present study. Number of replicates in each analysis is given below.

JSd-1 (wt %)	Reporte d	Analyze d	Recover y	%RSD	JSd-1 (mg/kg)	Reporte d	Analyze d	Recover y	%RSD
SiO₂	66.55	66.54	100	7.22	Ba	520	509.6	98.0	7.35
Al₂O₃	14.65	14.17	96.7	2.31	Cr	21.5	20.26	94.2	0.88
TiO₂	0.64	0.64	100	0.07	V	76.0	73.38	96.6	1.85
Fe₂O₃	5.06	5.03	99.5	1.00	Ni	7.04	6.62	94.0	0.30
MnO	0.09	0.09	99.6	0.33	Cu	22.0	21.81	99.1	0.13
MgO	1.81	1.81	99.9	0.66	Zn	96.5	96.07	99.6	0.30
CaO	3.03	3.03	99.8	4.40	Pb	12.9	12.66	98.1	0.17
Na₂O	2.73	2.72	99.9	1.58	Th	4.44	4.25	95.7	0.13
K₂O	2.18	2.17	99.2	0.40	Sr	340	321.7	94.6	12.94
P₂O₅	0.12	0.12	100	0.12	Rb	67.4	66.22	98.2	0.83
					Y	14.8	14.53	98.2	0.19
					Zr	132	129.8	98.3	1.56
					Nb	11.1	10.47	94.3	0.45
					Sc	10.9	10.77	98.8	0.09
Replicate s	2				3				

MAG -1 (mg/kg)	Reported	Analyzed	Recovery	%RSD
Ba	480	452.0	94.2	19.80
Cr	97.0	95.60	98.6	0.99
V	140	137.8	98.4	1.56
Ni	53.0	51.30	96.8	1.20
Cu	30.0	28.00	93.3	1.41
Zn	130	126.9	97.6	2.19
Pb	24.0	22.73	94.7	0.90
Th	12.0	11.40	95.0	0.42
Sr	150	147.6	98.4	1.70
Rb	150	142.6	95.0	5.23
Y	28.0	26.70	95.4	0.92
Zr	130	126.2	97.1	2.69
Nb	12.0	11.81	98.4	0.13
Sc	17.0	16.30	95.9	0.49
Replicates	3			

Table 4: Correlation coefficient matrix of terrigenous and excess part of Al, Mn and Fe (in wt%) with the trace metals (in mg/kg) (n = 35). Values with significance level >99% are in bold letters.

	Al (ex)	Al terri	Mn (ex)	Mn terri	Fe (ex)	Fe terri	Ba	Cr	V	Ni	Cu	Zn	Pb	Th	Sr	Rb	Y	Zr	Nb	Sc	
Al (ex)	1																				
Al terri	0.10	1																			
Mn (ex)	0.76	0.18	1																		
Mn terri	0.25	0.94	0.35	1																	
Fe (ex)	0.82	0.42	0.85	0.53	1																
Fe terri	0.25	0.97	0.29	0.98	0.52	1															
Ba	0.69	0.34	0.59	0.41	0.76	0.44	1														
Cr	0.53	0.52	0.43	0.52	0.67	0.55	0.70	1													
V	0.75	0.62	0.69	0.69	0.87	0.70	0.83	0.80	1												
Ni	0.78	0.58	0.80	0.67	0.86	0.67	0.73	0.72	0.95	1											
Cu	0.59	0.44	0.84	0.53	0.80	0.50	0.65	0.64	0.83	0.89	1										
Zn	0.04	0.17	0.10	0.12	0.07	0.12	-0.11	0.27	0.18	0.25	0.30	1									
Pb	0.46	0.65	0.41	0.67	0.62	0.70	0.56	0.63	0.80	0.75	0.70	0.31	1								
Th	0.74	0.49	0.64	0.54	0.76	0.54	0.56	0.65	0.85	0.88	0.75	0.25	0.63	1							
Sr	0.81	-0.06	0.67	0.10	0.58	0.08	0.49	0.28	0.52	0.60	0.41	0.01	0.10	0.63	1						
Rb	0.70	0.48	0.53	0.48	0.72	0.51	0.54	0.64	0.81	0.80	0.64	0.26	0.62	0.93	0.55	1					
Y	0.62	0.42	0.67	0.46	0.76	0.44	0.43	0.58	0.74	0.77	0.74	0.35	0.55	0.90	0.52	0.85	1				
Zr	0.78	0.48	0.66	0.54	0.74	0.54	0.56	0.63	0.84	0.89	0.73	0.26	0.61	0.96	0.70	0.90	0.80	1			
Nb	-0.35	0.26	-0.24	0.14	-0.02	0.18	-0.01	0.14	0.05	-0.08	0.14	0.12	0.45	-0.08	-0.70	0.00	0.04	-0.22	1		
Sc	0.56	0.75	0.46	0.74	0.71	0.77	0.59	0.75	0.89	0.84	0.68	0.29	0.82	0.80	0.23	0.83	0.70	0.79	0.23	1	

Table 5: Score matrix of the varimax rotated factors for the surface sediment samples under study.

Major Ox	Factor 1	Factor 2	Trace El	Factor 1	Factor 2	Factor 3	Factor 4
SiO ₂	2.5942	-1.6730	Cr	0.6219	0.0040	-0.0295	0.4479
TiO ₂	0.0050	0.0058	V	0.7151	-0.0142	-0.3487	0.1355
Al ₂ O ₃	-0.3620	-0.1396	Ni	1.0207	0.1525	-1.9275	-1.1353
Fe ₂ O ₃	-0.1325	0.0141	Cu	2.6016	0.1163	-0.8906	-1.0169
MnO	-0.1138	-0.0663	Zn	1.6040	-1.4234	0.5832	2.5069
MgO	-0.2167	-0.0832	Pb	0.2933	-0.7682	0.1953	0.4734
CaO	-1.6706	-2.6565	Th	0.1154	-0.0456	-0.0548	0.0513
Na ₂ O	-0.5120	0.3362	Sr	-1.2319	-0.4844	-2.9941	1.5118
K ₂ O	-0.0809	0.0033	Rb	0.7104	-0.2662	-0.0451	0.5459
P ₂ O ₅	-0.0401	-0.0098	Y	0.5331	-0.1353	-0.1171	-0.1110
			Zr	-0.5224	-3.3194	0.0325	-1.5329
			Nb	0.0687	-0.0379	0.0345	0.0205
			Sc	0.1876	-0.0193	-0.0718	-0.0275
Percentage variance			Percentage variance				
	99.27	0.48		85.15	7.27	5.08	1.38
Total Variance			Total Variance				
	99.75%			98.88%			

Table 6: Correlation coefficient matrix of the important geochemical parameters of the studied samples (n = 69). Values with significance level >99% are in bold letters.

	Mn*	Mn(ex)	Al(ex)	SiO ₂ (ex)	Fe(ex)	Terri %	Al/Ti
Mn*	1						
Mn(ex)	0.36	1					
Al(ex)	0.33	0.53	1				
SiO₂(ex)	-0.61	-0.46	-0.73	1			
Fe(ex)	0.18	0.51	0.69	-0.62	1		
Terri %	-0.11	0.47	0.38	-0.30	0.60	1	
Al/Ti	0.41	0.37	0.85	-0.64	0.46	-0.09	1

List of Figures:

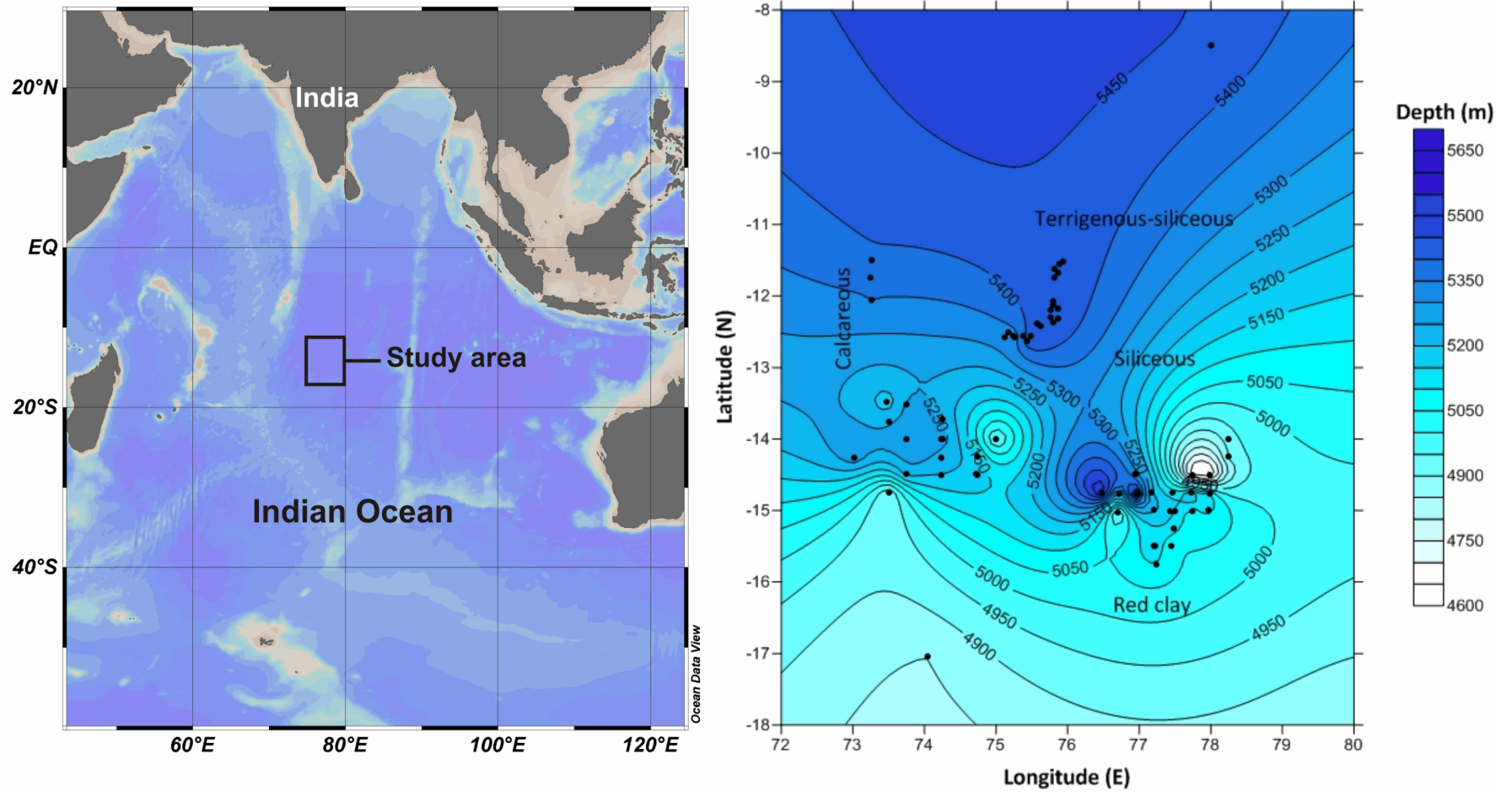


Figure 1: Study area in the Indian Ocean with the station locations (69), bathymetry of the area and different sediment types encountered.

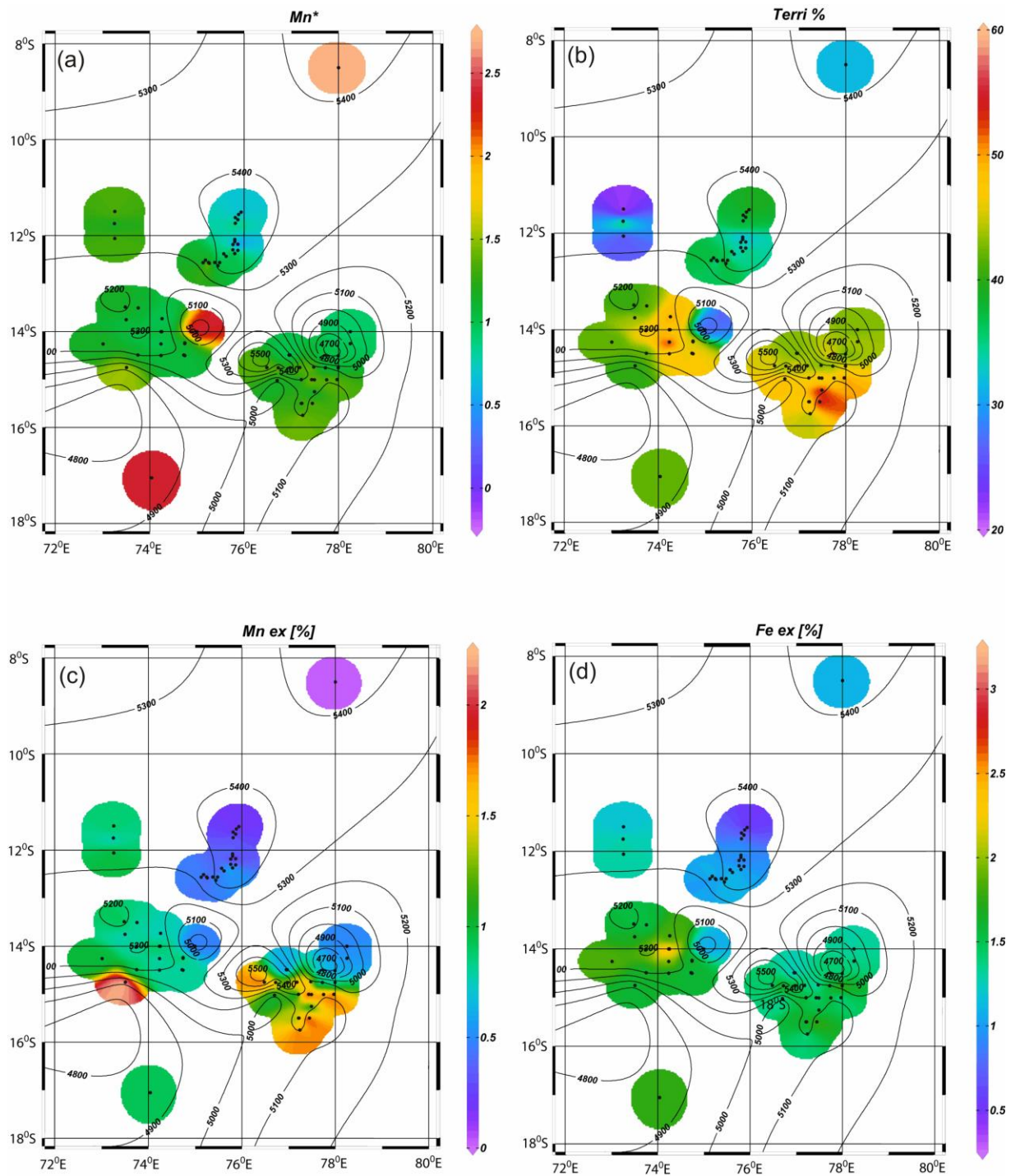
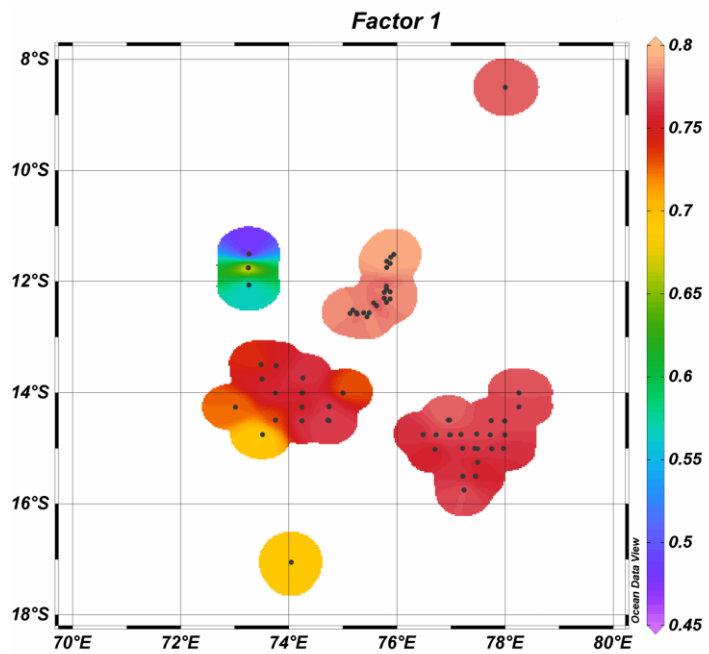
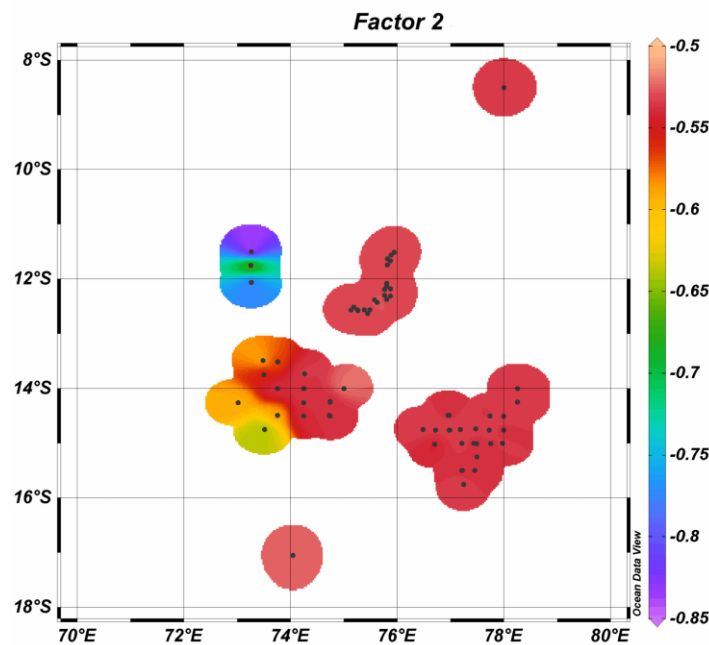


Figure 2: Distribution of (a) Mn* (redox indicator), (b) Terri% (terrigenous percentage), (c) Mn ex (non-terrigenous/excess Mn) and (d) Fe ex (non-terrigenous/excess Fe) contents of the sediment samples. Both excess Mn and Fe are in wt %. Bathymetry of the study area is provided in each map as lines with corresponding depths in numbers.



(a)



(b)

Figure 4: Distribution of the Q-mode factor analysis data for major element oxides, against the station locations of the sediment samples under study. (a) Factor 1 contains highest loadings of SiO_2 with 99.27% of the total variance and (b) Factor 2 represents negative relation with CaO concentrations of the samples which means CaO concentration is highest where Factor 2 is lowest.

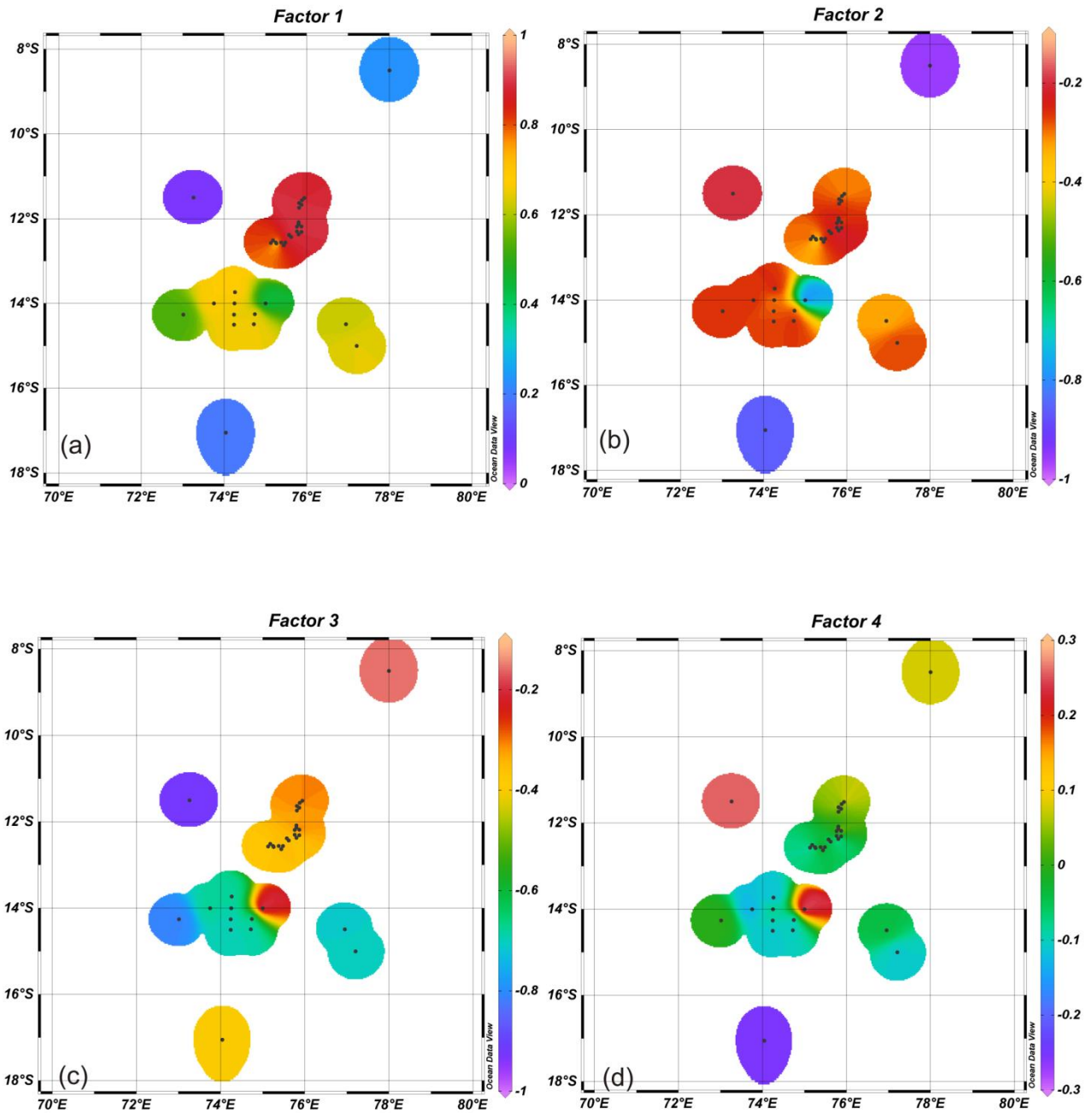


Figure 5: Distribution of the Q-mode factor analysis data for trace elements, against the station locations of the sediment samples under study. (a) Factor 1 containing higher loadings of Cu, Zn and Ni with 85.5% of the total variance, (b) Factor 2 containing higher loadings of Zr and Zn with 7.27% of the total variance, (c) Factor 3 containing higher loadings of Sr and Ni with 5.08% of the total variance and (d) Factor 4 containing higher loadings of Zn and Sr with 1.38% of the total variance.

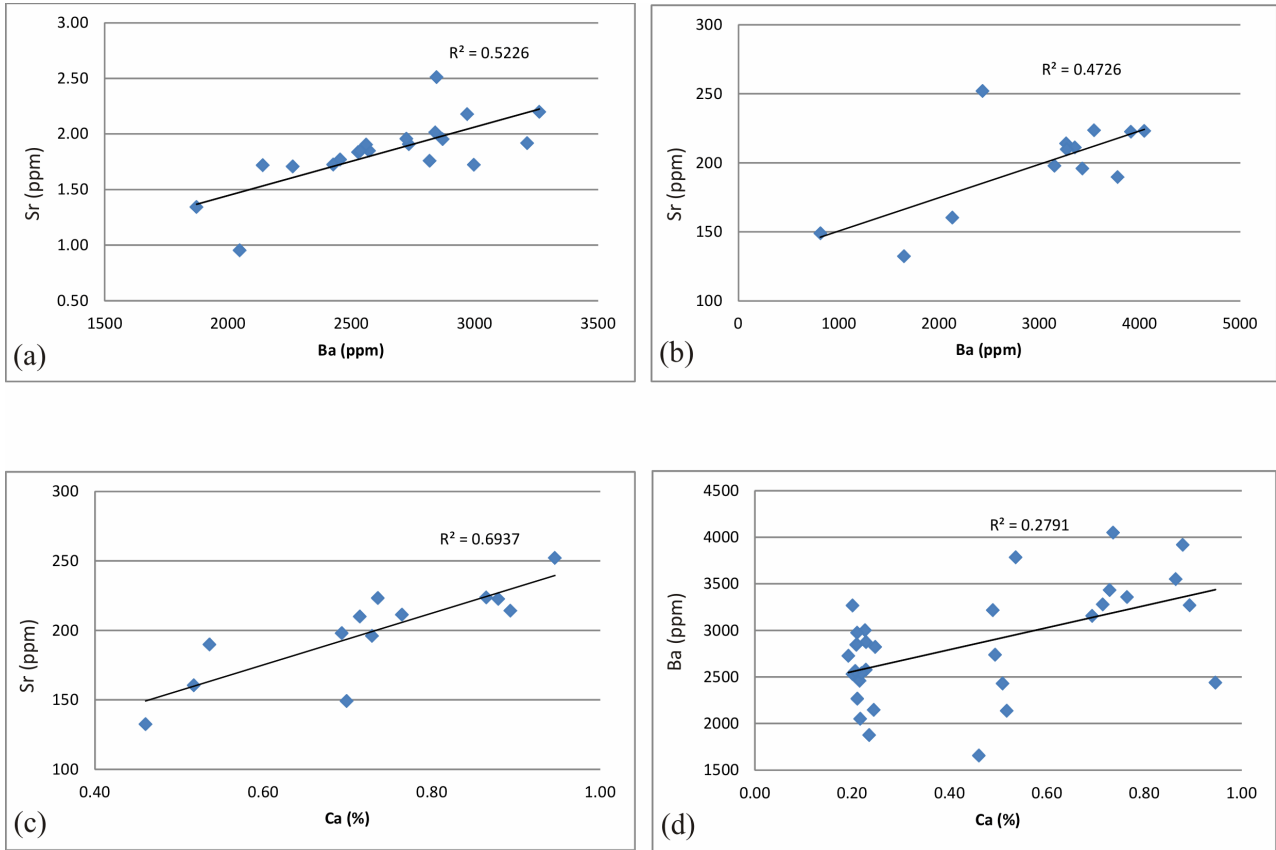


Figure 6: Sr vs Ba for the (a) T-S sediment and siliceous high productivity zone ($R = 0.72$, $n = 20$), (b) siliceous low productivity zone and red clay sediment ($R = 0.68$, $n = 13$), Sr vs Ca for the (c) siliceous low productivity zone and red clay sediment ($R = 0.83$, $n = 13$) and (d) Ba vs Ca for $n = 32$, $R = 0.53$. Calcareous sediment samples are excluded from the calculations as their very high Ca and Sr contents are affecting the overall trend of the studied samples.

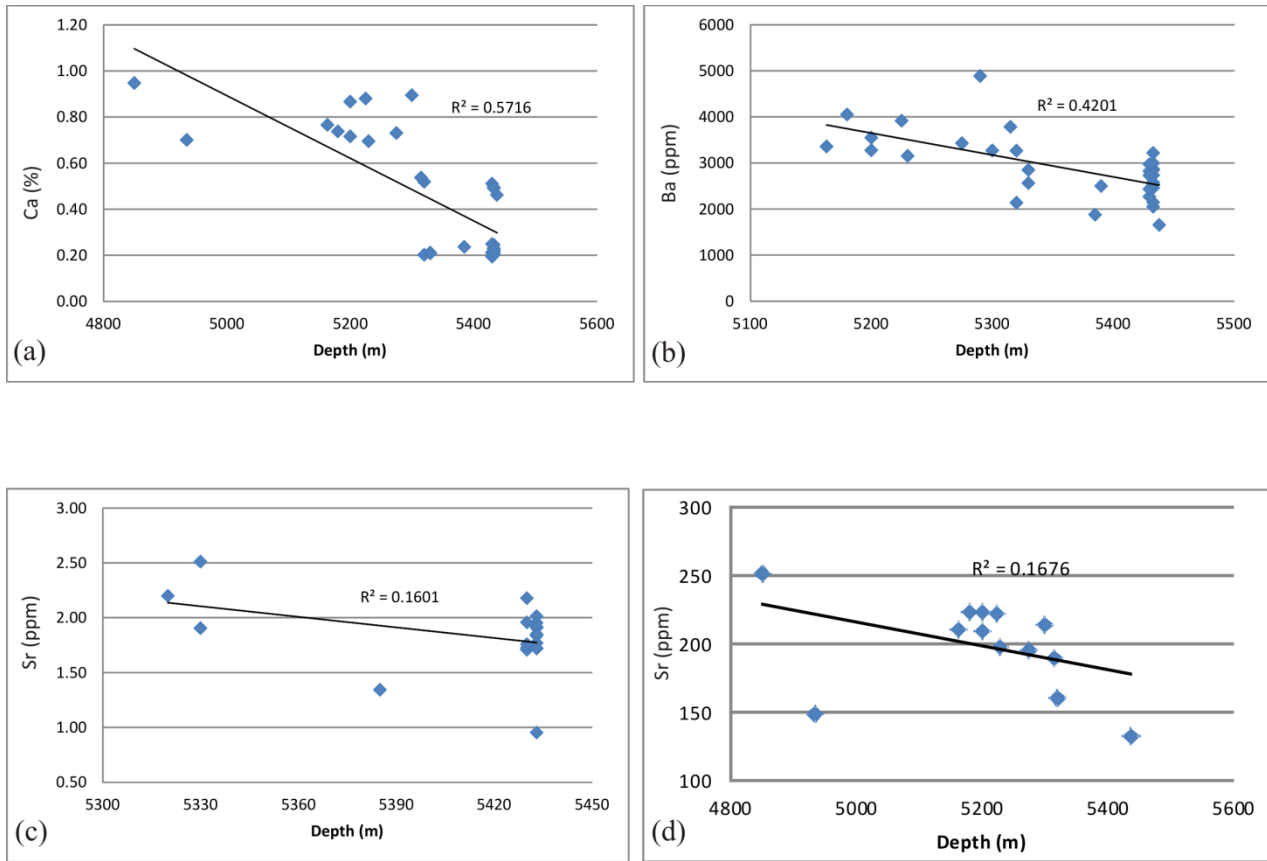


Figure 7: Antipathetic relationships observed from the depth vs concentration graphs of (a) Ca ($R = -0.75$) and (b) Ba ($R = -0.65$) of all the samples, (c) Sr of T-S sediment and siliceous high productivity zone ($R = -0.40$, $n = 20$) and (d) Sr of siliceous low productivity zone and red clay sediment ($R = -0.41$, $n = 13$). Calcareous sediment samples are excluded from the calculations as their very high Ca and Sr contents are affecting the overall trend of the studied samples.